

Supporting information

Two-dimensional metal-organic nanosheets composed of single-molecule magnets: structural modulation and enhanced magnetism utilizing steric hindrance effect.

Ikumi Aratani,^a Yoji Horii,*^a Yoshinori Kotani,^b Hitoshi Osawa^b, Hajime Tanida^c, Toshiaki Ina^b, Takeshi Watanabe^b, Yohko F. Yano^d, Akane Mizoguchi^a, Daisuke Takajo^e and Takashi Kajiwara^a

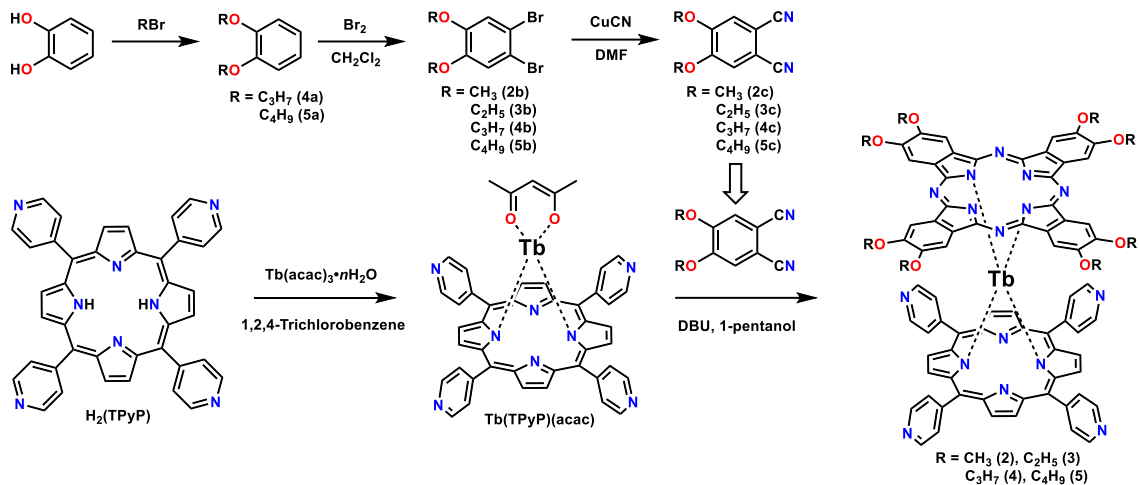
^a*Graduate School of Humanity and Science, Nara Women's University, Kitauoya-Higashimachi, Nara 630-8506, Japan.*

^b*SPring-8/JASRI, Kouto, Sayo, Hyogo 679-5198, Japan.*

^c*Materials Sciences Research Center, Sector of Nuclear Science Research, Japan Atomic Energy Agency, Sayo, Hyogo 679-5148, Japan*

^d*Department of Physics, Kindai University, 3-4-1 Kowakae, Higashiosaka City, Osaka 577-8502, Japan*

^e*Research Center for Thermal and Entropic Science, Graduate School of Science, Osaka University, 1-1 Machikaneyama-cho, Toyonaka, Osaka 560-0043, Japan.*



Scheme S1. Synthesis of SMMs.

Synthesis of 1,2-dimethoxy-4,5-dibromobenzene (2b)

The mixture of 1,2-dimethoxybenzene (Tokyo Chemical Industry Co., Ltd., 7.65 mL, 0.060 mol), I₂ (one bead, ca. 50 mg) and dried CH₂Cl₂ (150 mL) was cooled to 0 °C using ice bath. The mixture of Br₂ (7.1 mL) and dried CH₂Cl₂ (50 mL) was added dropwise over 1 hour. The reaction mixture was stirred for 22 hours at room temperature. The residual Br₂ was quenched using Na₂SO₃ aq., and the solution was neutralized using NaHCO₃ aq. The CH₂Cl₂ layer was washed for several times with the water using the separately funnel. After drying the CH₂Cl₂ layer over MgSO₄, the CH₂Cl₂ was removed using rotary evaporator. The white solid was completely dissolved in the hot isopropanol (150 mL) and kept at -20 °C to afford the white crystalline solid of **2b** (70%).

¹H NMR (400 MHz, CDCl₃, TMS): δ 7.051 (s, 2H, H_{Ar}), 3.844 (s, 6H, CH₃-O).

Synthesis of 1,2-dimethoxy-4,5-dicyanobenzene (2c)

The mixture of 1,2-dimethoxy-4,5-dibromobenzene (8.6 g, 0.030 mol), CuCN (7.9 g, 0.090 mol) and dried DMF (120 mL) was refluxed for 5 hours under N₂ atmosphere. After cooling to room temperature, NH₃ aq. (28%, 300 mL) was added and stirred for 3 days. The precipitate was collected by vacuum filtration, washed with water, and dried under the vacuum. The soxhlet extraction was carried out using Et₂O for 3 days, and the white solid was collected by vacuum filtration. Recrystallization using CH₂Cl₂ and Et₂O afforded the white crystalline solid of **2c** (38%).

¹H NMR (400 MHz, CDCl₃): δ 7.152 (s, 2H, H_{Ar}), 3.974 (s, 6H, CH₃-O).

Synthesis of 1,2-diethoxy-4,5-dibromobenzene (3b)

The mixture of 1,2-diethoxybenzene (Tokyo Chemical Industry Co., Ltd., 9.86 g, 0.060 mol), I₂ (one bead, ca. 50 mg) and dried CH₂Cl₂ (150 mL) was cooled to 0 °C using ice bath. The mixture of Br₂

(7.1 mL) and dried CH_2Cl_2 (50 mL) was added dropwise over 1 hour. The reaction mixture was stirred for 22 hours at room temperature. The residual Br_2 was quenched using Na_2SO_3 aq., and the solution was neutralized using NaHCO_3 aq. The CH_2Cl_2 layer was washed for several times with the water using the separately funnel. After drying the CH_2Cl_2 layer over MgSO_4 , the CH_2Cl_2 was removed using rotary evaporator. The product was obtained as the colourless oil of **3b** (77%).

^1H NMR (400 MHz, CDCl_3): δ 7.062 (s, 2H, H_{Ar}), 4.0 (q, 4H, $\text{CH}_3\text{-CH}_2\text{-O}$), 1.4 (t, 6H, $\text{CH}_3\text{-CH}_2$).

Synthesis of 1,2-diethoxy-4,5-dicyanobenzene (**3c**)

The mixture of 1,2-diethoxy-4,5-dibromobenzene (9.9 g, 0.030 mol), CuCN (8.0 g, 0.090 mol) and dried DMF (120 mL) was refluxed for 5 hours under N_2 atmosphere. After cooling to room temperature, NH_3 aq. (28%, 300 mL) was added and stirred for 3 days. The precipitate was collected by vacuum filtration, washed with water, and dried under the vacuum. The soxhlet extraction was carried out using Et_2O for 4 days, and the white solid was collected by vacuum filtration. Purification with the silica gel column chromatography using CH_2Cl_2 as the eluent and recrystallization using CH_2Cl_2 and Et_2O afforded the white crystalline solid of **3c** (41%).

^1H NMR (400 MHz, CDCl_3): δ 7.119 (s, 2H, H_{Ar}), 4.15 (q, 4H, $\text{CH}_3\text{-CH}_2\text{-O}$), 1.51 (t, 6H, $\text{CH}_3\text{-CH}_2$).

Synthesis of 1,2-dipropoxybenzene (**4a**)

The mixture of catechol (8.25 g, 0.075 mol), K_2CO_3 (41.6 g, 0.3 mol), dried acetone (83 mL), and 1-bromopropane (15 mL, 0.166 mol) was refluxed for 48 hours under N_2 atmosphere. After cooling to room temperature, the K_2CO_3 was removed by vacuum filtration and washed with CH_2Cl_2 to extract the product. The reaction product was purified with the silica gel column chromatography using CH_2Cl_2 as the eluent, and the colourless oil of **4a** was obtained (84%).

^1H NMR (400 MHz, CDCl_3): δ 6.889 (s, 2H, H_{Ar}), 4.0 (t, 4H, $\text{CH}_2\text{-CH}_2\text{-O}$), 1.8 (sext., 4H, $\text{CH}_3\text{-CH}_2\text{-CH}_2$), 1.0 (t, 6H, $\text{CH}_3\text{-CH}_2$).

Synthesis of 1,2-dipropoxy-4,5-dibromobenzene (**4b**)

The mixture of 1,2-dipropoxybenzene (12.26 g, 0.063 mol), I_2 (one bead, ca. 50 mg) and dried CH_2Cl_2 (150 mL) was cooled to 0 °C using ice bath. The mixture of Br_2 (7.1 mL) and dried CH_2Cl_2 (50 mL) was added dropwise over 1 hour. The reaction mixture was stirred for 22 hours at room temperature. The residual Br_2 was quenched using Na_2SO_3 aq., and the solution was neutralized using NaHCO_3 aq. The CH_2Cl_2 layer was washed for several times with the water using the separately funnel. After drying the CH_2Cl_2 layer over MgSO_4 , the CH_2Cl_2 was removed using rotary evaporator. Purification with the silica gel column chromatography using hexane/ethyl acetate (9:1) as the eluent afforded the white solid of **4b** (79%).

^1H NMR (400 MHz, CDCl_3): δ 7.064 (s, 2H, H_{Ar}), 3.9 (t, 4H, $\text{CH}_2\text{-CH}_2\text{-O}$), 1.8 (sext., 4H, $\text{CH}_3\text{-CH}_2\text{-CH}_2$).

CH_2), 1.0 (t, 6H, $\text{CH}_3\text{-CH}_2$).

Synthesis of 1,2-dipropoxy-4,5-dicyanobenzene (**4c**)

The mixture of 1,2-dipropoxy-4,5-dibromobenzene (10.53 g, 0.030 mol), CuCN (8.0 g, 0.090 mol) and dried DMF (120 mL) was refluxed for 5 hours under N_2 atmosphere. After cooling to room temperature, NH_3 aq. (28%, 300 mL) was added and stirred for 3 days. The precipitate was collected by vacuum filtration, washed with water, and dried under the vacuum. The soxhlet extraction was carried out using Et_2O for 3 days, and the white solid was collected by vacuum filtration. Purification with the silica gel column chromatography using CH_2Cl_2 as the eluent and the recrystallization using CH_2Cl_2 and Et_2O afforded the crystalline solid of **4c** (78%).

^1H NMR (400 MHz, CDCl_3): δ 7.115 (s, 2H, H_{Ar}), 4.0 (t, 4H, $\text{CH}_2\text{-CH}_2\text{-O}$), 1.9 (sext., 4H, $\text{CH}_3\text{-CH}_2\text{-CH}_2$), 1.1 (t, 6H, $\text{CH}_3\text{-CH}_2$).

Synthesis of 1,2-dibutoxybenzene (**5a**)

The mixture of catechol (15 g, 0.136 mol), KOH (18.1 g, 0.27 mol), Aliquot 336 (1 mL) and 1-bromobutane (29 mL, 0.27 mol) was refluxed for 5 hours. After cooling to room temperature, the residue was extracted with CH_2Cl_2 , washed with H_2O using separatory funnel, and dried over MgSO_4 . After the removal of CH_2Cl_2 using rotary evaporator, the oil was purified using vacuum distillation (91%).

Synthesis of 1,2-dibutoxy-4,5-dibromobenzene (**5b**)

The mixture of 1,2-dibutoxybenzene (12 g, 0.054 mol) and dried CH_2Cl_2 (150 mL) was cooled to 0 °C using ice bath. The mixture of Br_2 (6.5 mL) and dried CH_2Cl_2 (15 mL) was added dropwise over 0.5 hour. The reaction mixture was stirred for 30 hours at room temperature. The residual Br_2 was quenched using Na_2SO_3 aq., and the solution was neutralized using NaHCO_3 aq. The CH_2Cl_2 layer was washed for several times with the water using the separately funnel. After drying the CH_2Cl_2 layer over MgSO_4 , the CH_2Cl_2 was removed using rotary evaporator. Purification with the silica gel column chromatography using hexane/ethyl acetate (4:1) as the eluent afforded the colourless oil of **5b** (95%).

Synthesis of 1,2-dibutoxy-4,5-dicyanobenzene (**5c**)

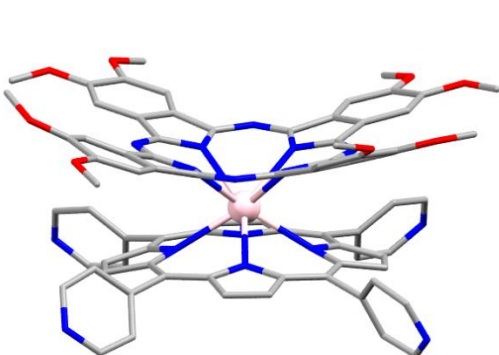
The mixture of 1,2-dibutoxy-4,5-dibromobenzene (11.7 g, 0.034 mol), CuCN (7.5 g, 0.084 mol) and dried DMF (100 mL) was refluxed for 5 hours under N_2 atmosphere. After cooling to room temperature, NH_3 aq. (28%, 300 mL) was added and stirred for 60 hours. The precipitate was collected by vacuum filtration, washed with water, and dried under the vacuum. Purification with the silica gel column chromatography using CHCl_3 as the eluent and the recrystallization using CHCl_3 and Et_2O afforded the crystalline solid of **5c** (42%).

¹H NMR (400 MHz, CDCl₃): δ 7.115 (s, 2H, H_{Ar}), 4.06 (t, 4H, CH₂-CH₂-O), 1.84 (quin., 4H, CH₂-CH₂-CH₂), 1.51 (sext., 4H, CH₃-CH₂-CH₂), 1.0 (t, 6H, CH₃-CH₂).

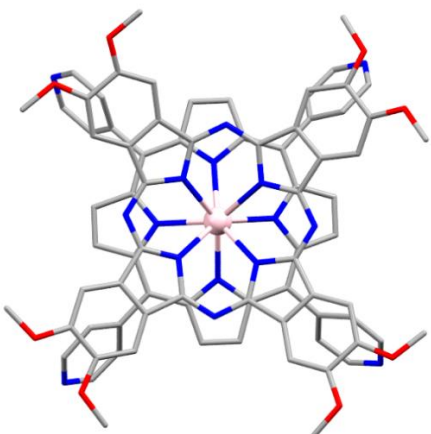
Table S1. Crystalline cell parameters for **1-5**. The parameters for **1** were taken from the literature.¹

	1	2	3	4	5
<i>T</i> / K	153	153	153	153	153
Formula	C ₇₄ H ₄₄ Cl ₄ N ₁₆ Tb	C ₈₂ H ₆₀ Cl ₄ N ₁₆ O ₈ Tb	C ₉₄ H ₈₅ Cl ₆ N ₁₆ O ₈ Tb	C _{100.79} H _{98.79} Cl _{3.58} N ₁₆ O ₈ Tb	C _{105.47} H _{106.94} Cl _{2.94} N ₁₆ O ₈ Tb
Crystal system	Triclinic	Monoclinic	Triclinic	Triclinic	Triclinic
Space group	<i>P</i> -1	<i>P</i> 2 ₁ / <i>n</i>	<i>P</i> -1	<i>P</i> -1	<i>P</i> -1
<i>Z</i>	2	4	2	2	2
<i>a</i> / Å	12.7976(5)	13.9287(4)	12.4898(2)	12.68090(10)	13.14280(10)
<i>b</i> / Å	14.0071(6)	18.9066(4)	16.8197(3)	17.4595(2)	17.69370(10)
<i>c</i> / Å	18.1335(7)	30.4607(9)	23.7164(5)	24.1597(2)	21.7886(2)
α / °	93.068(3)	90	71.843(2)	69.7820(10)	106.1290(10)
β / °	105.135(4)	92.075(3)	77.170(2)	75.3100(10)	103.3890(10)
γ / °	100.887(3)	90	73.3800(10)	70.6080(10)	94.4290(10)
<i>V</i> / Å ³	3063.1(2)	8016.4(4)	4487.75(16)	4676.06(9)	4680.46(7)
<i>ρ</i> / g cm ⁻³	1.581	1.407	1.434	1.383	1.412
GOF	1.035	1.012	1.059	1.049	1.041
<i>R</i> ₁ (gt)	0.0638	0.0558	0.0417	0.0460	0.0335
<i>wR</i> ₂ (gt)	0.1359	0.1146	0.0432	0.1231	0.0902
<i>R</i> ₁ (all)	0.0995	0.1082	0.0432	0.0501	0.0345
<i>wR</i> ₂ (ref)	0.1516	0.1330	0.1174	0.1259	0.0909
CCDC number	2205797	2293113	2293116	2293114	2293115

(a)



(b)



(c)

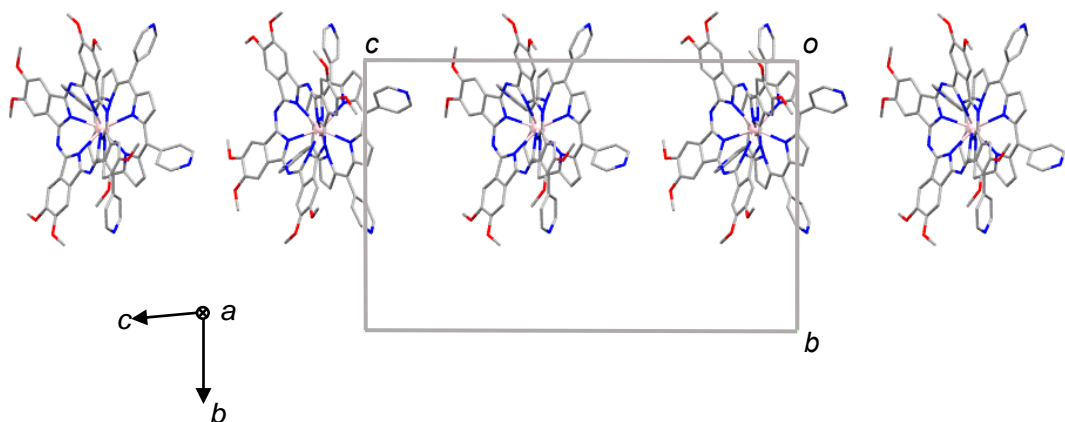


Fig. S1 Crystal structure of **2** at 153 K. (a) Side view, (b) top view and (c) crystal packing. Solvent molecules and hydrogen atoms are omitted for clarity. Tb pink; C grey; N blue; O red.

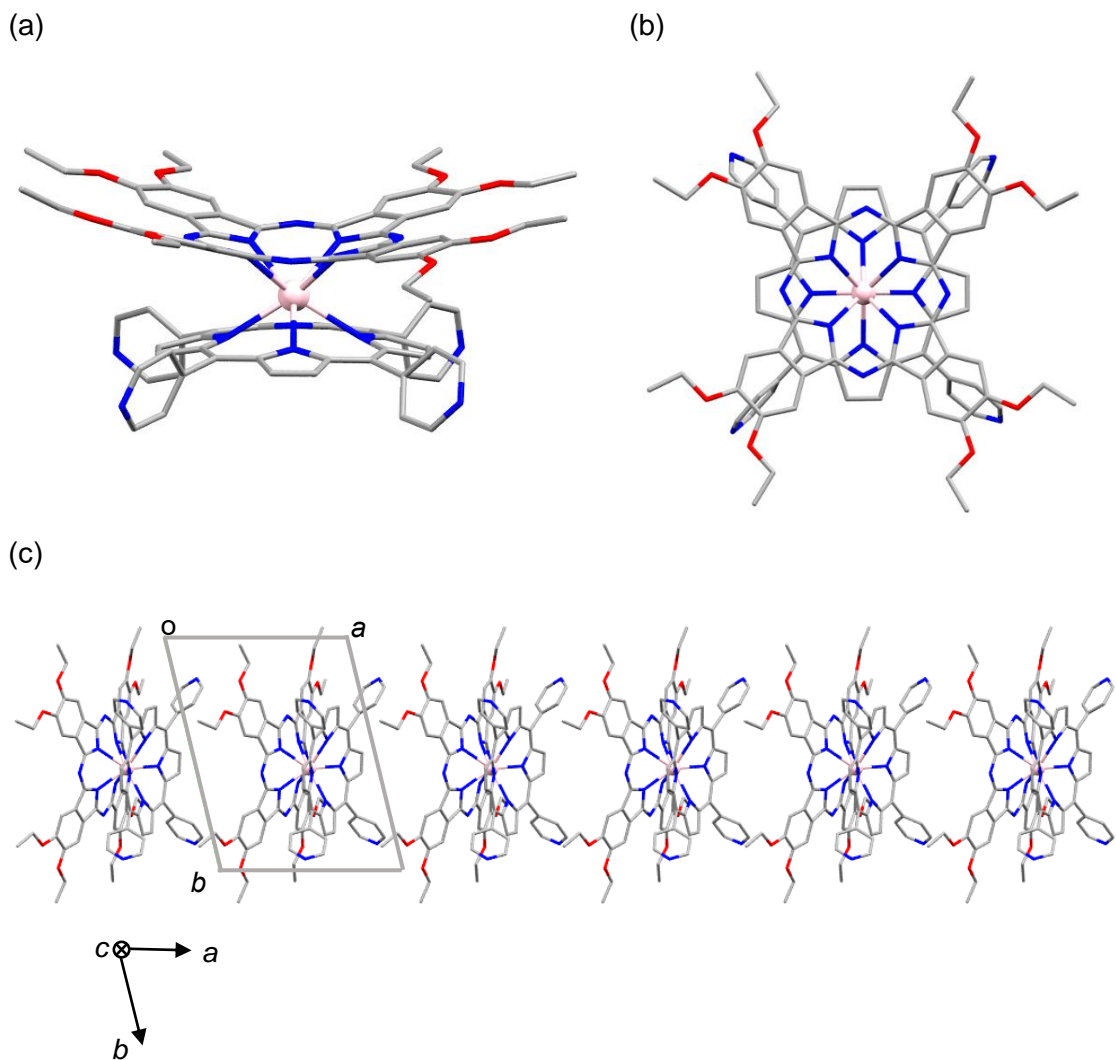


Fig. S2 Crystal structure of **3** at 153 K. (a) Side view, (b) top view and (c) crystal packing. Solvent molecules and hydrogen atoms are omitted for clarity. Tb pink; C grey; N blue; O red.

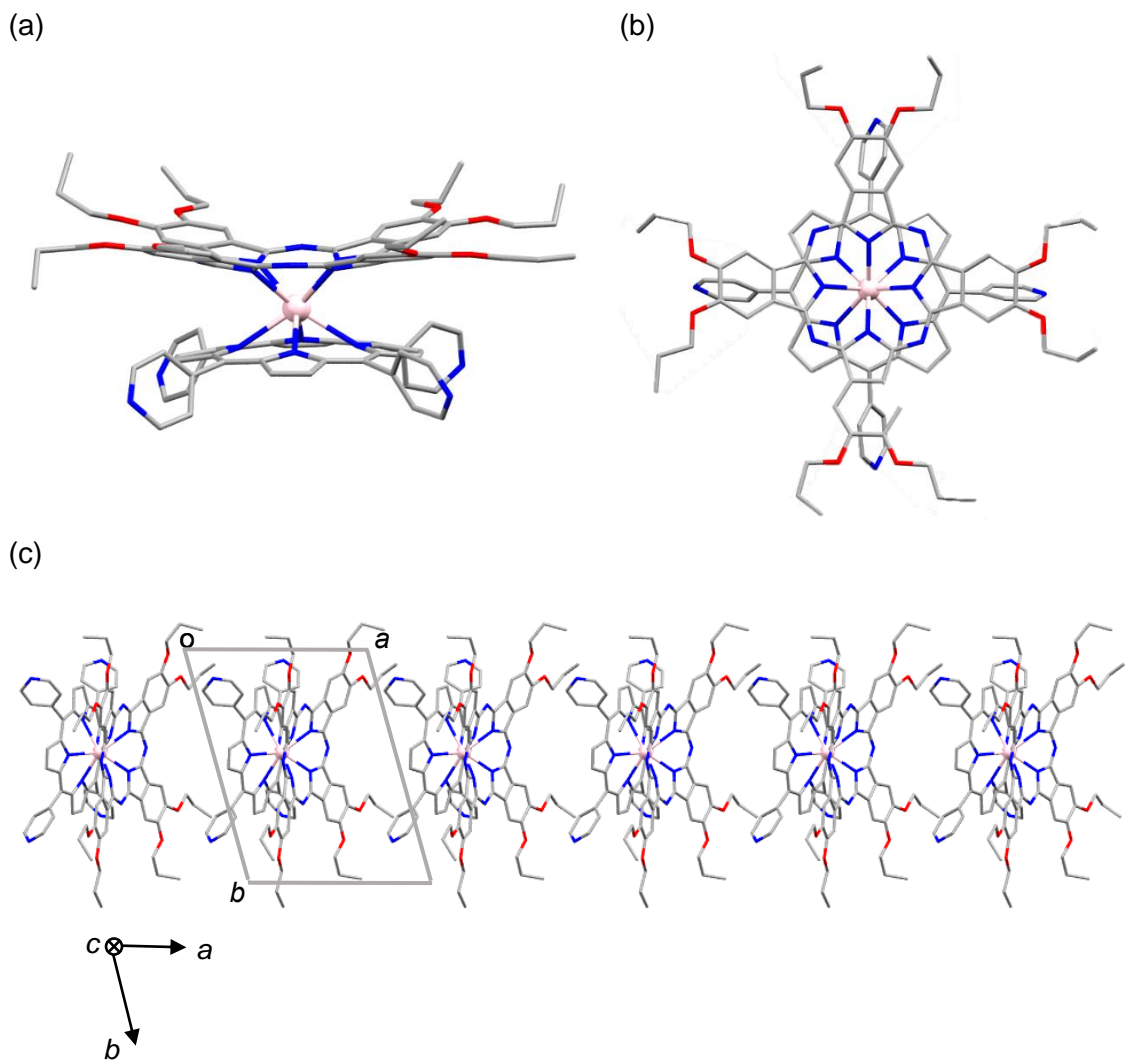


Fig. S3 Crystal structure of 4 at 153 K. (a) Side view, (b) top view and (c) crystal packing. Solvent molecules and hydrogen atoms are omitted for clarity. Tb pink; C grey; N blue; O red.

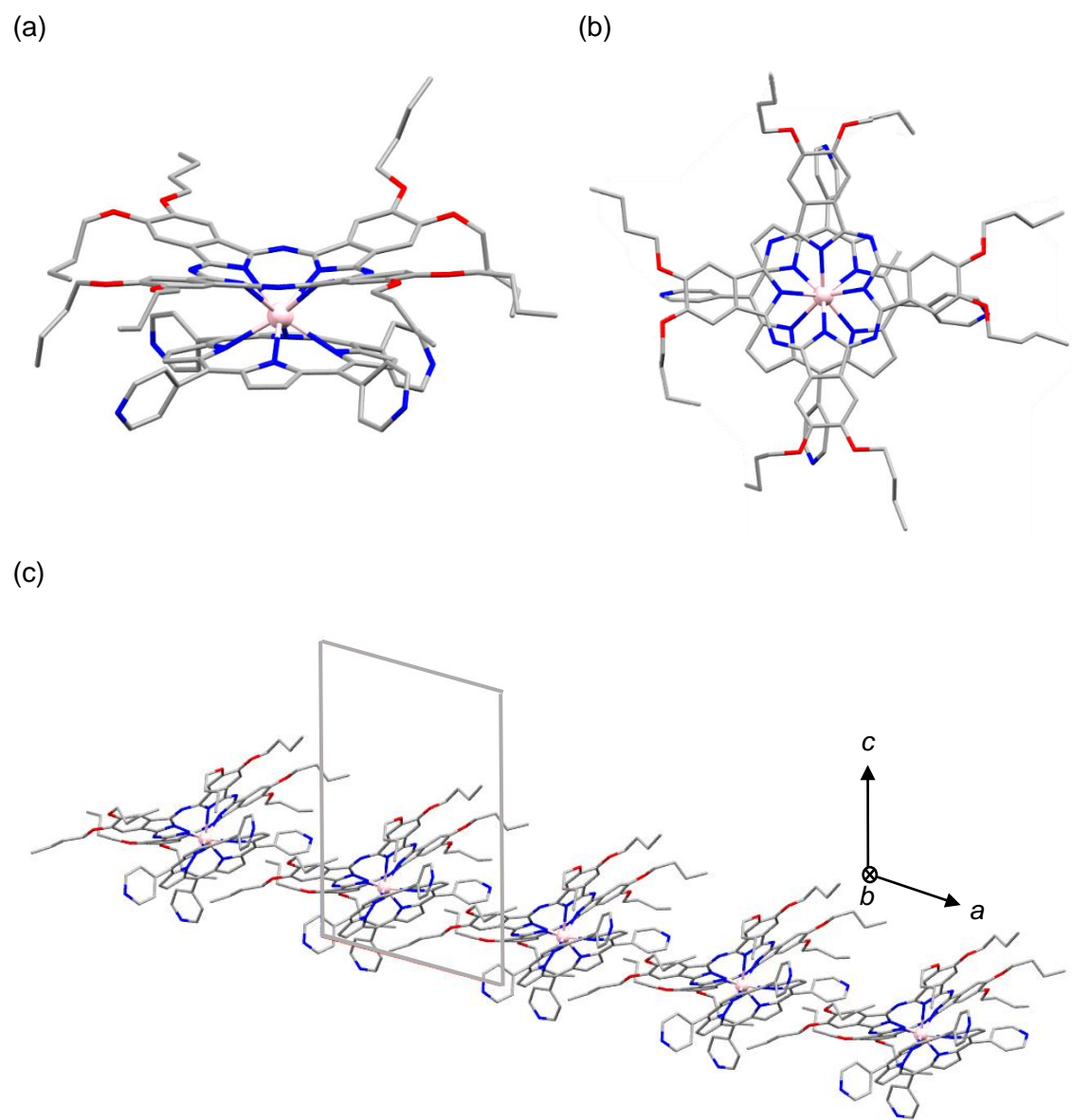


Fig. S4 Crystal structure of **5** at 153 K. (a) Side view, (b) top view and (c) crystal packing. Solvent molecules and hydrogen atoms are omitted for clarity. Tb pink; C grey; N blue; O red.

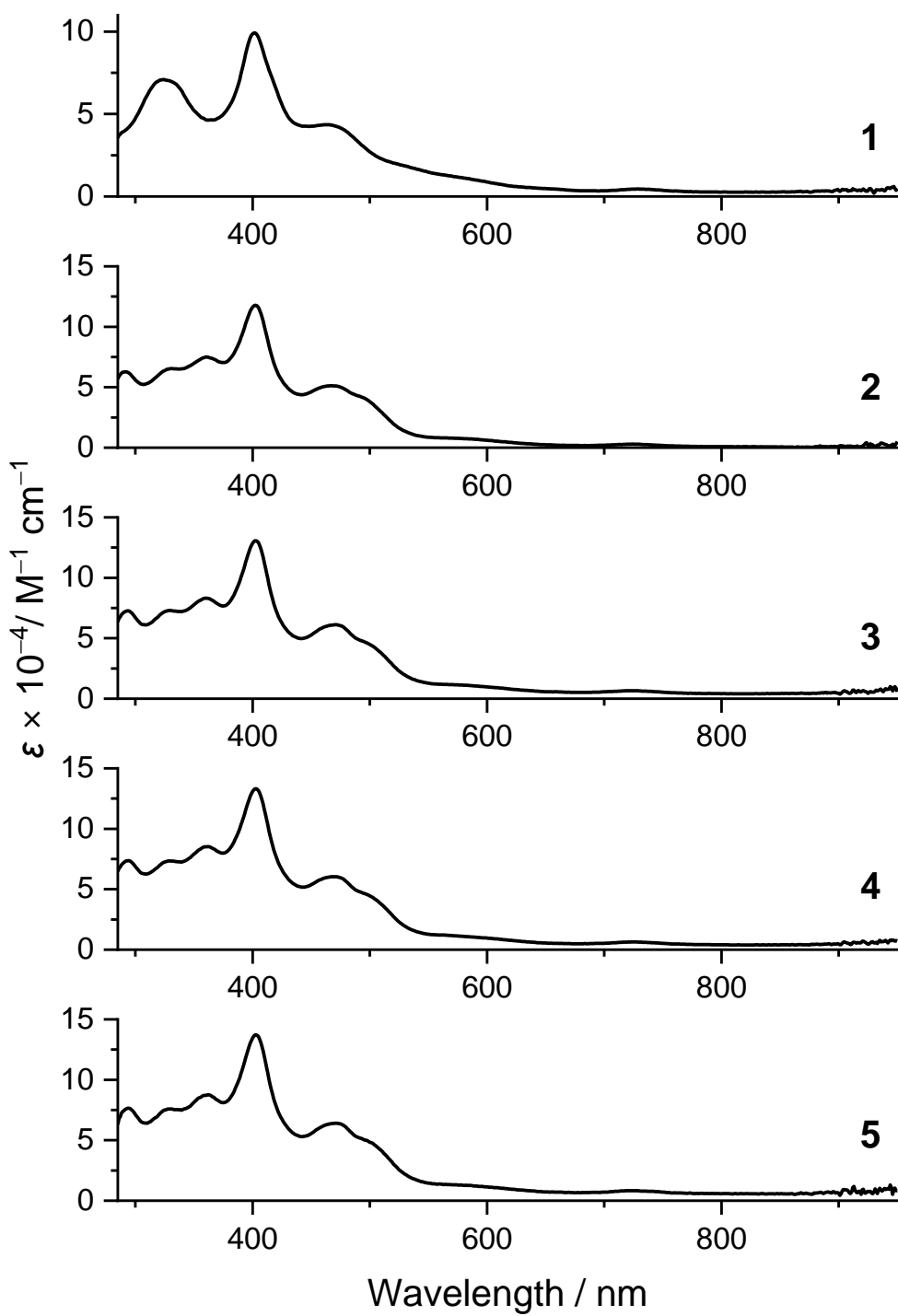


Fig. S5 UV-Vis-NIR spectra for **1-5** in toluene.

Table S2. Basis sets used for CASSCF-SOC calculations.

Atom	Basis set
Tb	SARC2-DKH-QZVP ²
Coordinating N	DKH-Def2-TZVP ³
Remaining atoms	DKH-Def2-SVP ³

Table S3. Mulliken charges on the coordinating N atoms.

	1	2	3	4	5
Pc	-0.7479	-0.7525	-0.7472	-0.7720	-0.7719
	-0.7506	-0.7770	-0.7493	-0.7642	-0.8377
	-0.7410	-0.7559	-0.7643	-0.7857	-0.7694
	-0.7337	-0.7550	-0.7669	-0.7676	-0.8138
Average	-0.7433	-0.7601	-0.7570	-0.7724	-0.7982
TPyP	-0.8556	-0.8436	-0.8520	-0.8585	-0.8493
	-0.8726	-0.8452	-0.8554	-0.7988	-0.9242
	-0.8498	-0.8472	-0.8518	-0.8593	-0.8610
	-0.8524	-0.8511	-0.8526	-0.7925	-0.9164
Average	-0.8576	-0.8468	-0.8530	-0.8273	-0.8877

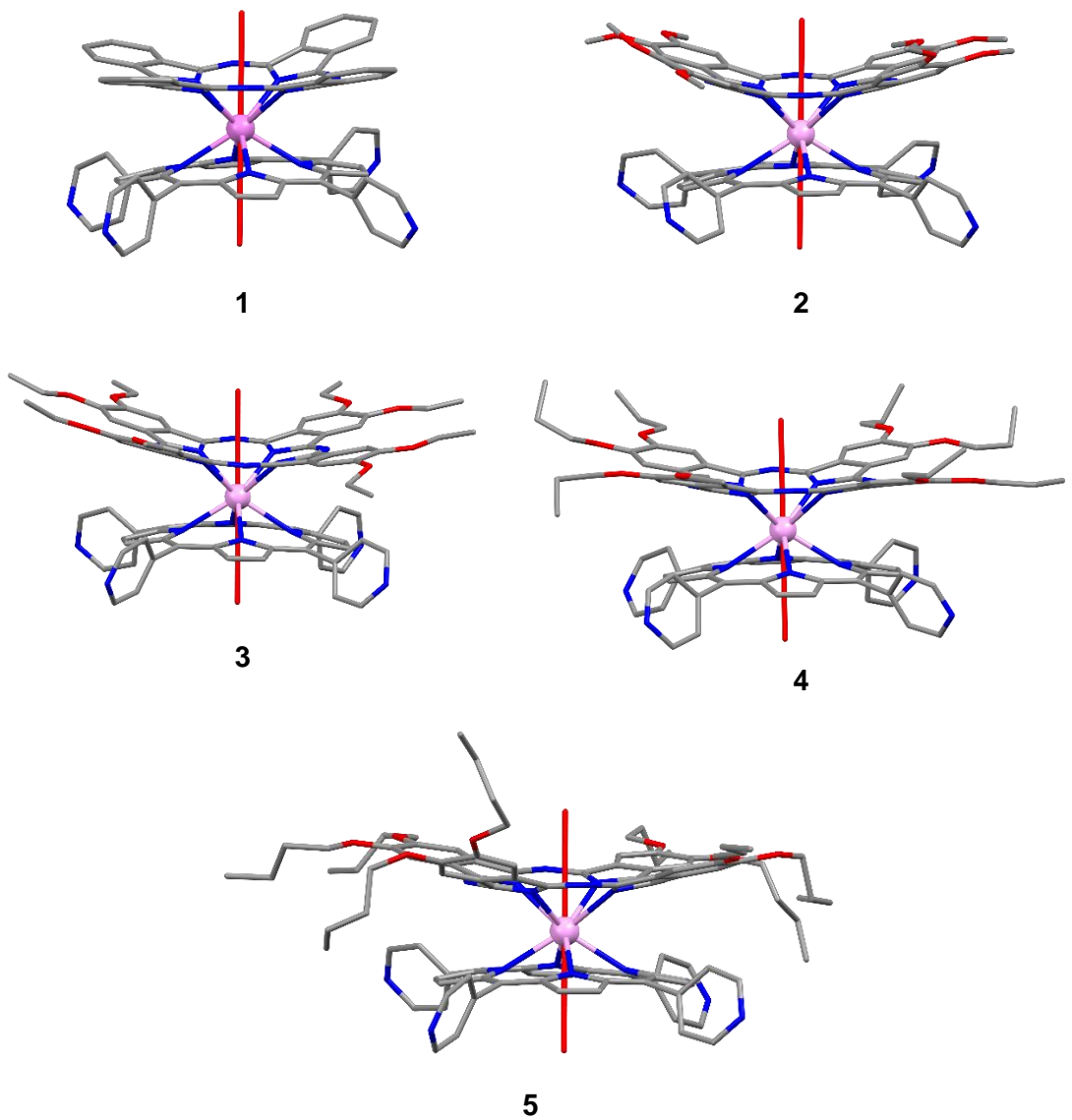


Fig. S6 Magnetic easy axis of the ground quasi-doublet states of **1-5** derived from CASSCF-SO calculations.

Table S4. Energy level and wavefunction composition (%) of the 7F_6 states of **2**.

Table S5. Energy level and wavefunction composition (%) of the 7F_6 states of **3**.

Table S6. Energy level and wavefunction composition (%) of the 7F_6 states of **4**.

Table S7. Energy level and wavefunction composition (%) of the 7F_6 states of **5**.

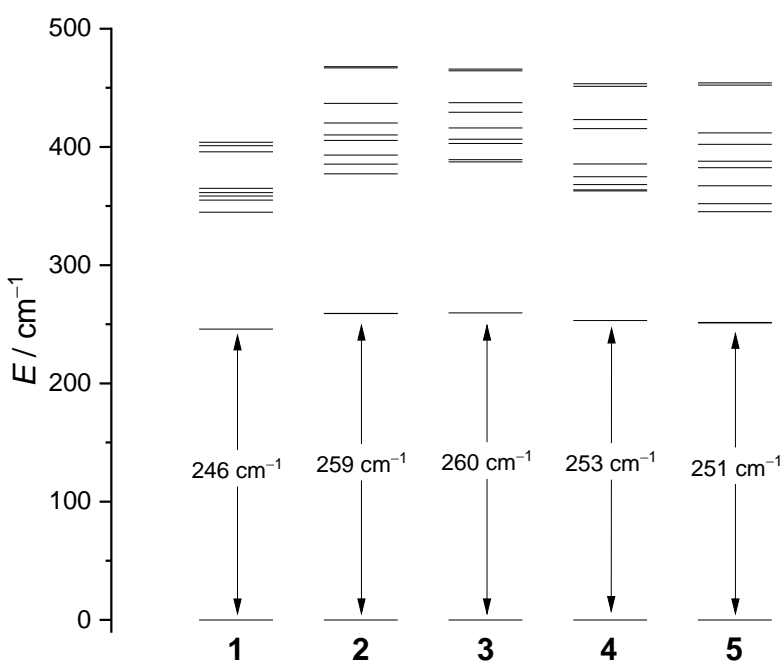


Fig. S7 Ligand-field energy diagram of **1-5** based on CASSCF-SO calculations.

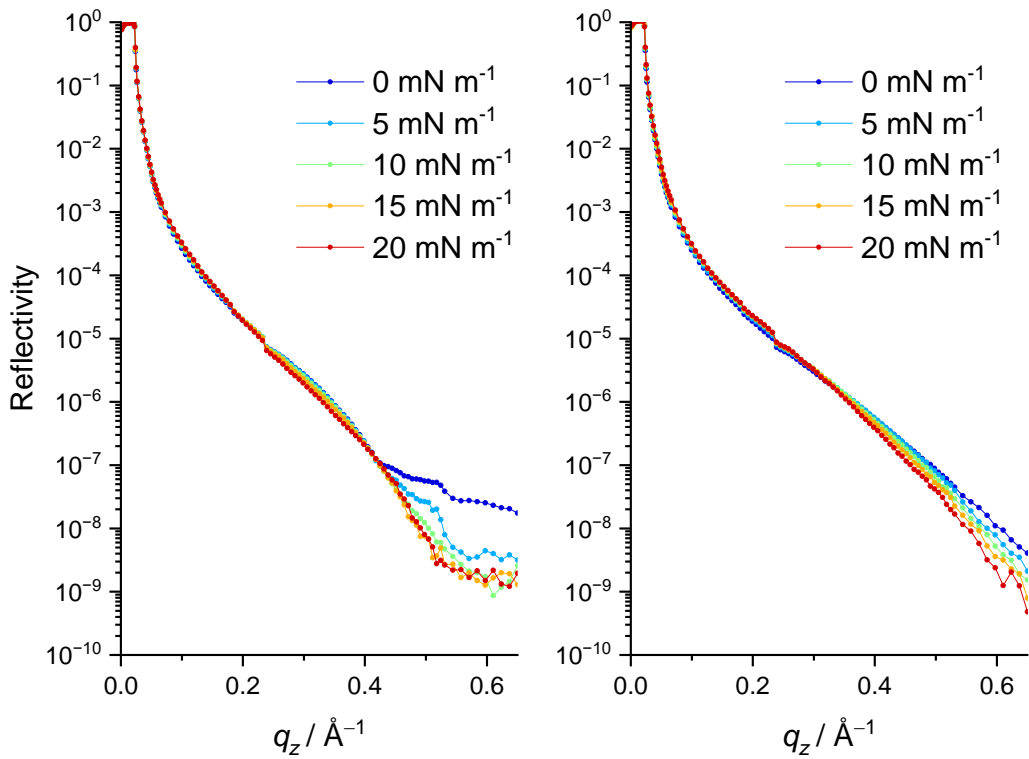


Fig. S8 X-ray reflectivity of **1** on ultra-pure water (left) and $\text{Na}_2[\text{PdCl}_4]$ aq. (right)

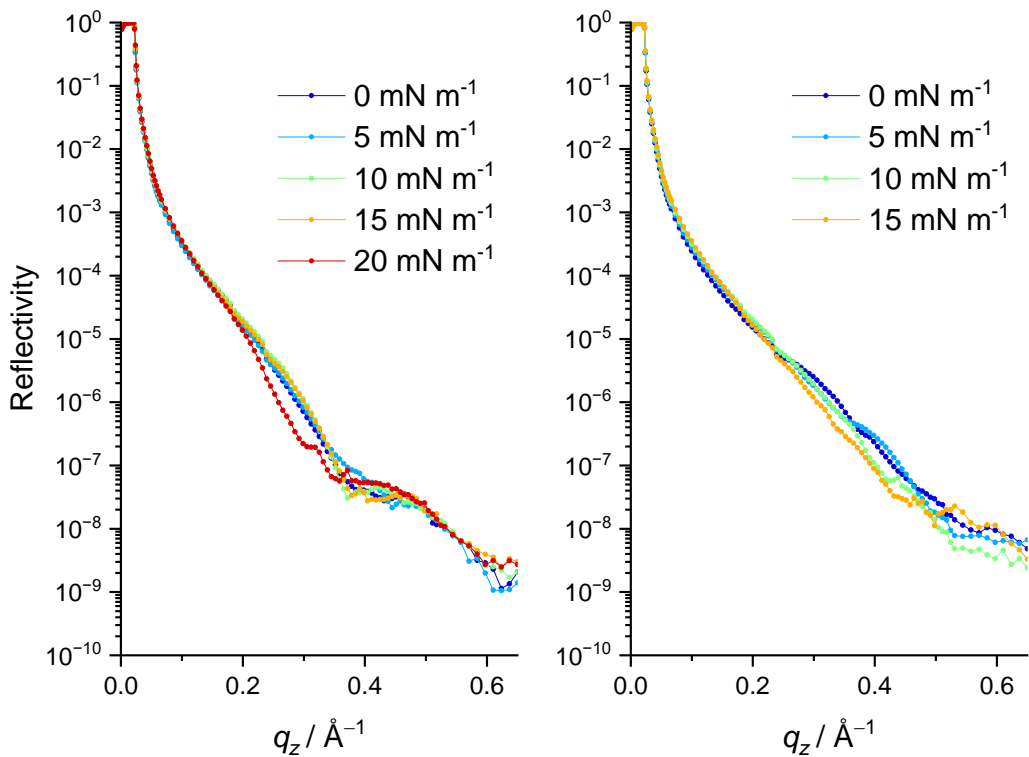


Fig. S9 X-ray reflectivity of **2** on ultra-pure water (left) and $\text{Na}_2[\text{PdCl}_4]$ aq. (right)

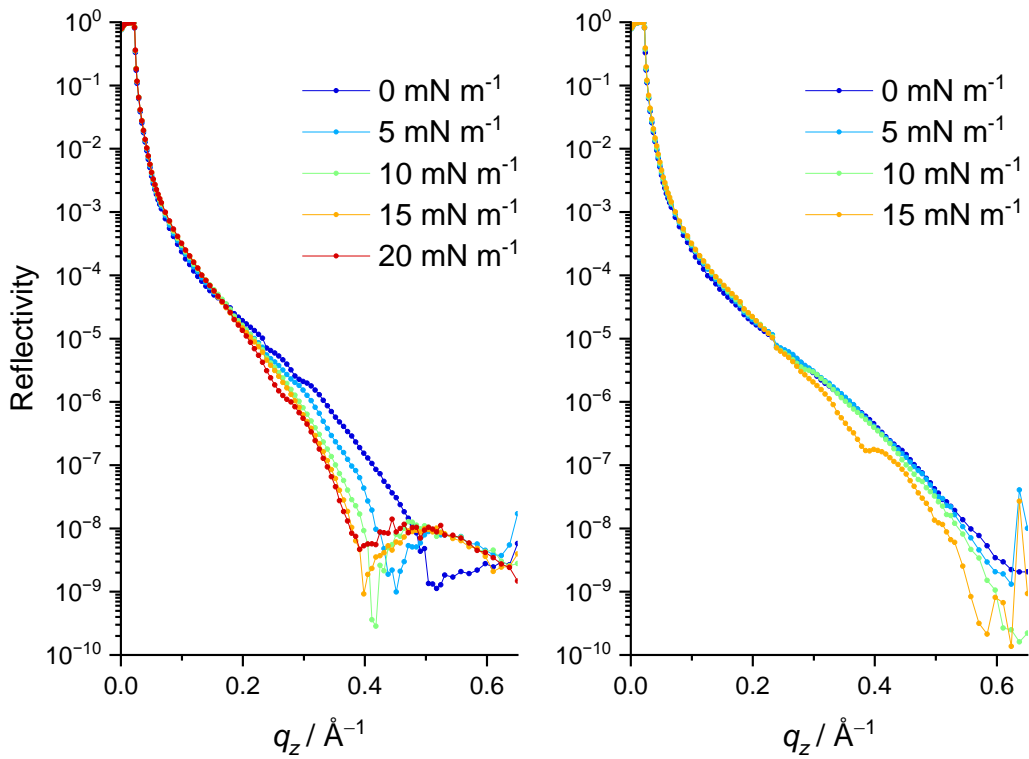


Fig. S10 X-ray reflectivity of **3** on ultra-pure water (left) and $\text{Na}_2[\text{PdCl}_4]$ aq. (right)

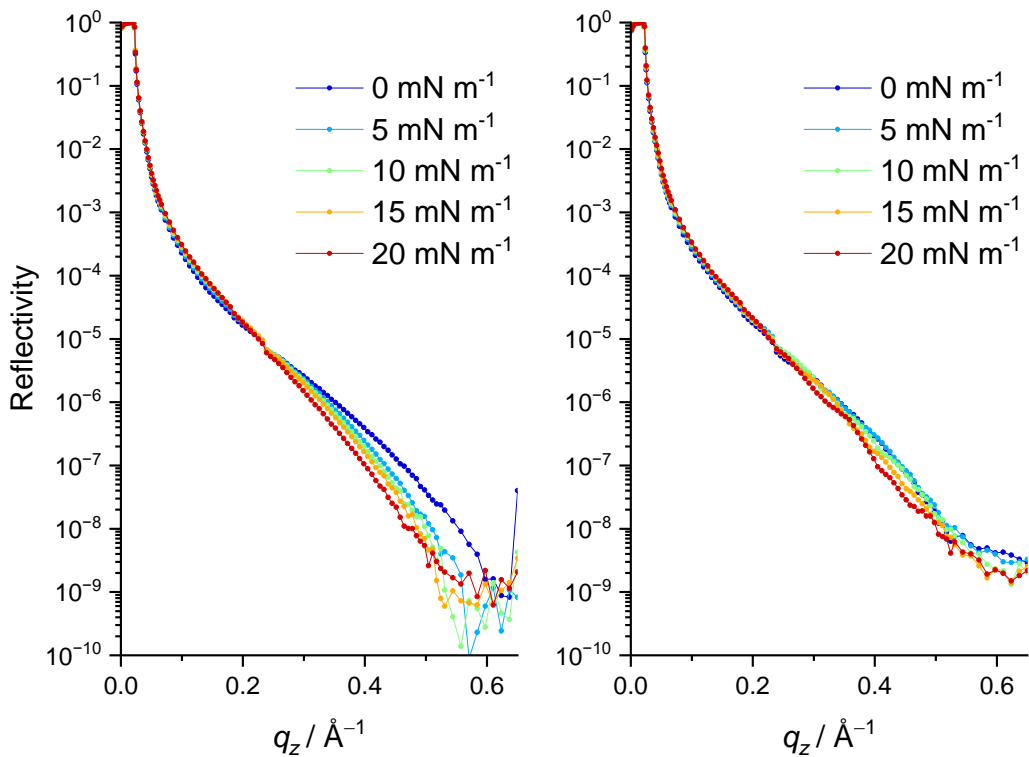


Fig. S11 X-ray reflectivity of **4** on ultra-pure water (left) and $\text{Na}_2[\text{PdCl}_4]$ aq. (right)

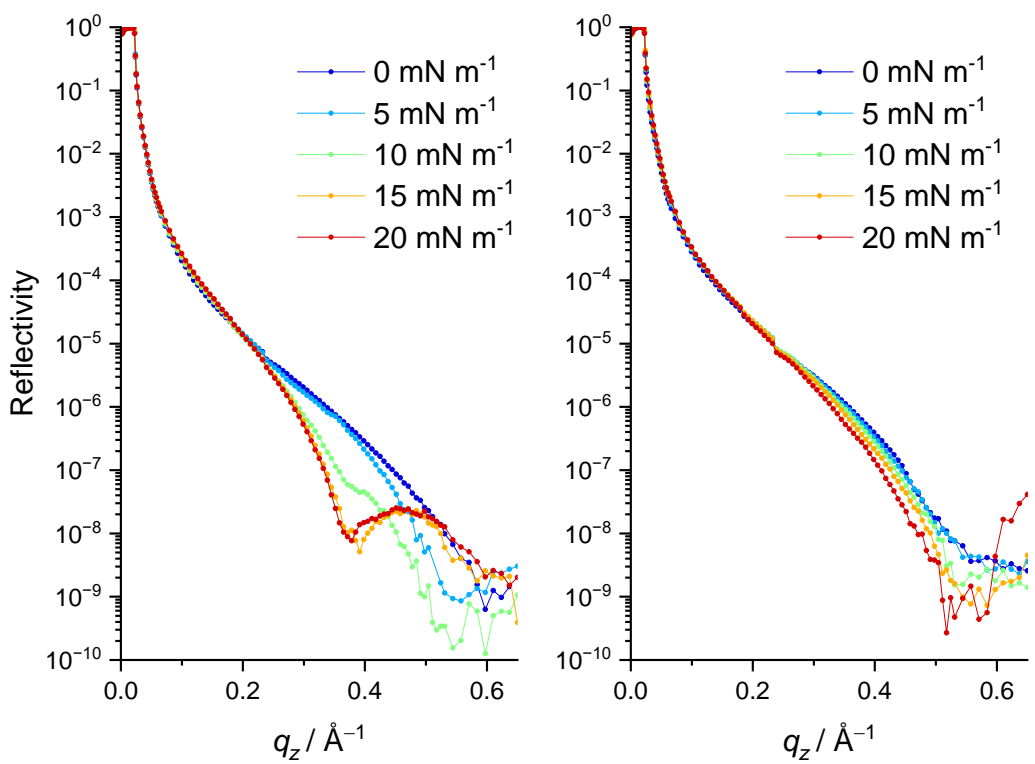


Fig. S12 X-ray reflectivity of **5** on ultra-pure water (left) and $\text{Na}_2[\text{PdCl}_4]$ aq. (right)

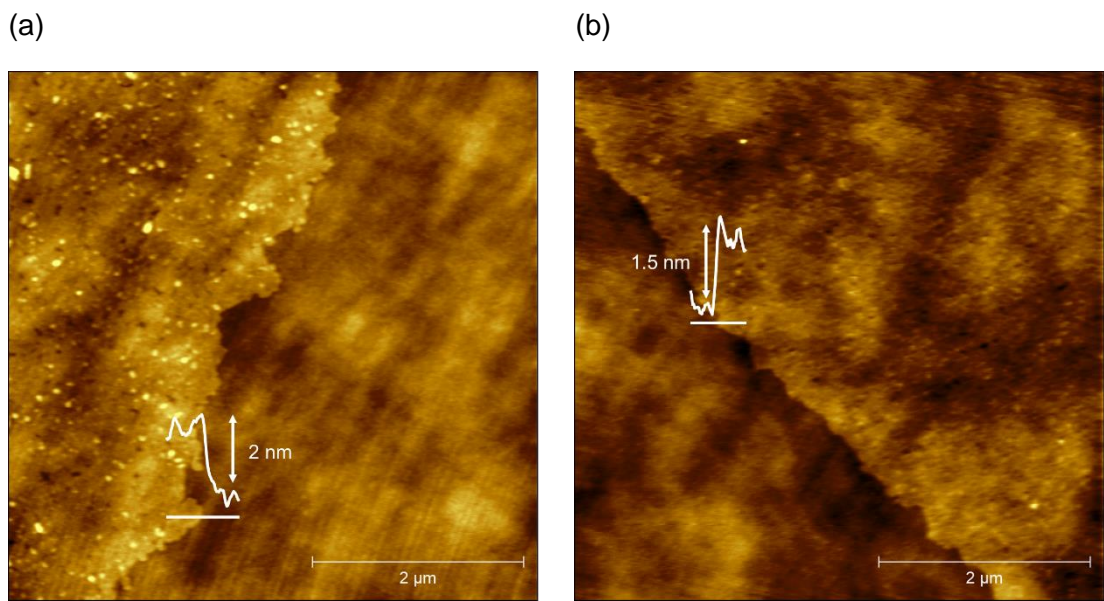


Fig. S13 AFM image of (a) $\mathbf{1}^{\text{aq}}$ and (b) $\mathbf{1}^{\text{Pd}}$ on the Si wafer.

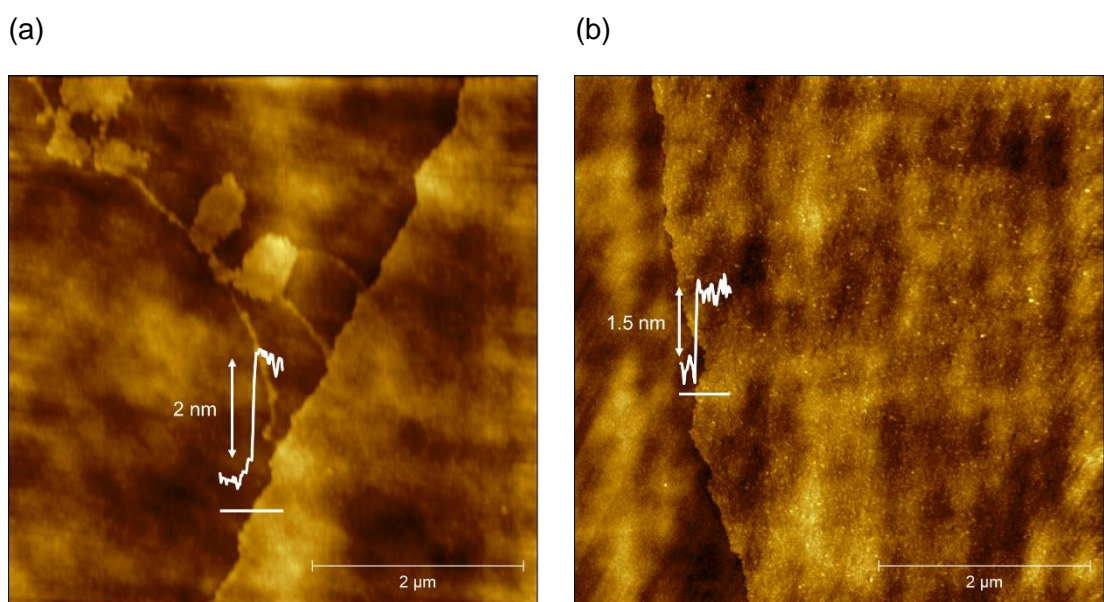


Fig. S14 AFM image of (a) $\mathbf{2}^{\text{aq}}$ and (b) $\mathbf{2}^{\text{Pd}}$ on the Si wafer.

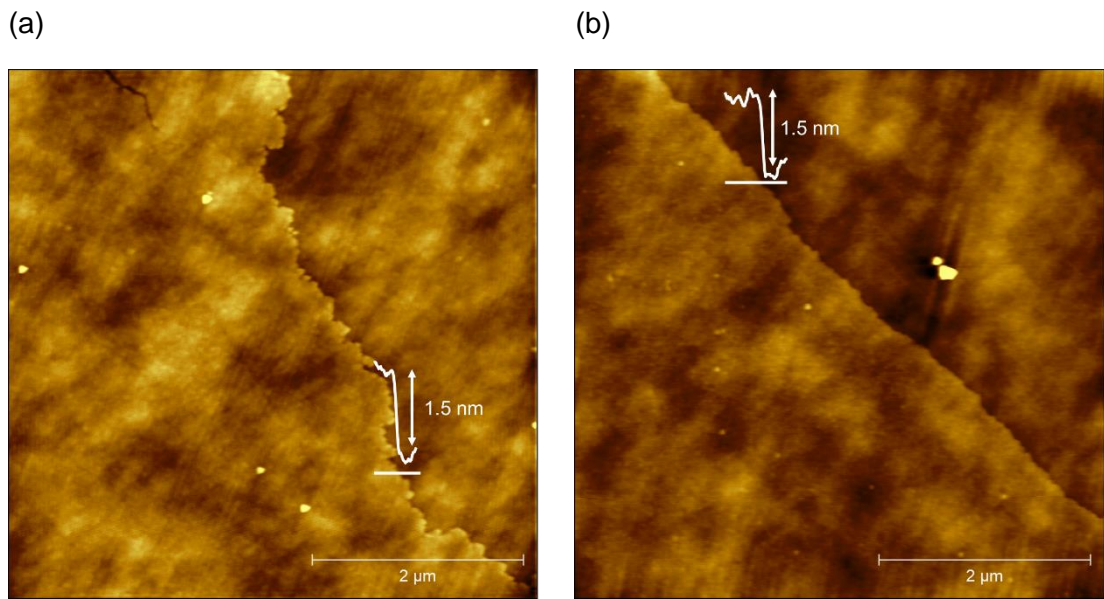


Fig. S15 AFM image of (a) 3^{aq} and (b) 3^{Pd} on the Si wafer.

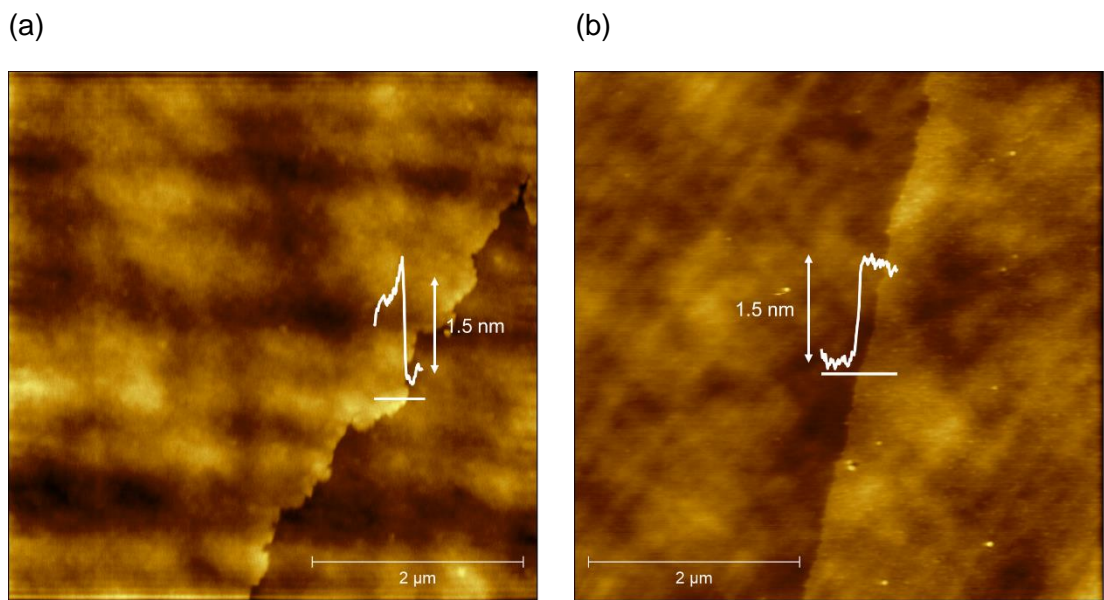
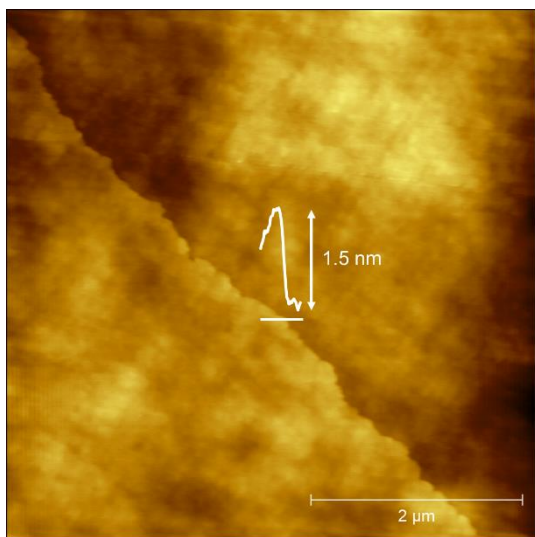


Fig. S16 AFM image of (a) 4^{aq} and (b) 4^{Pd} on the Si wafer.

(a)



(b)

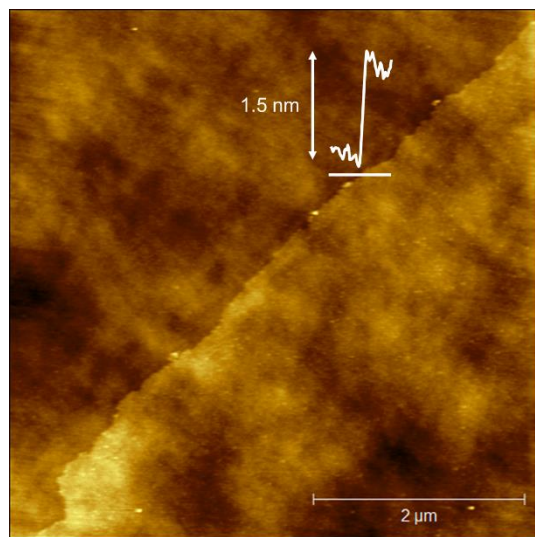


Fig. S17 AFM image of (a) **5^{aq}** and (b) **5^{Pd}** on the Si wafer.

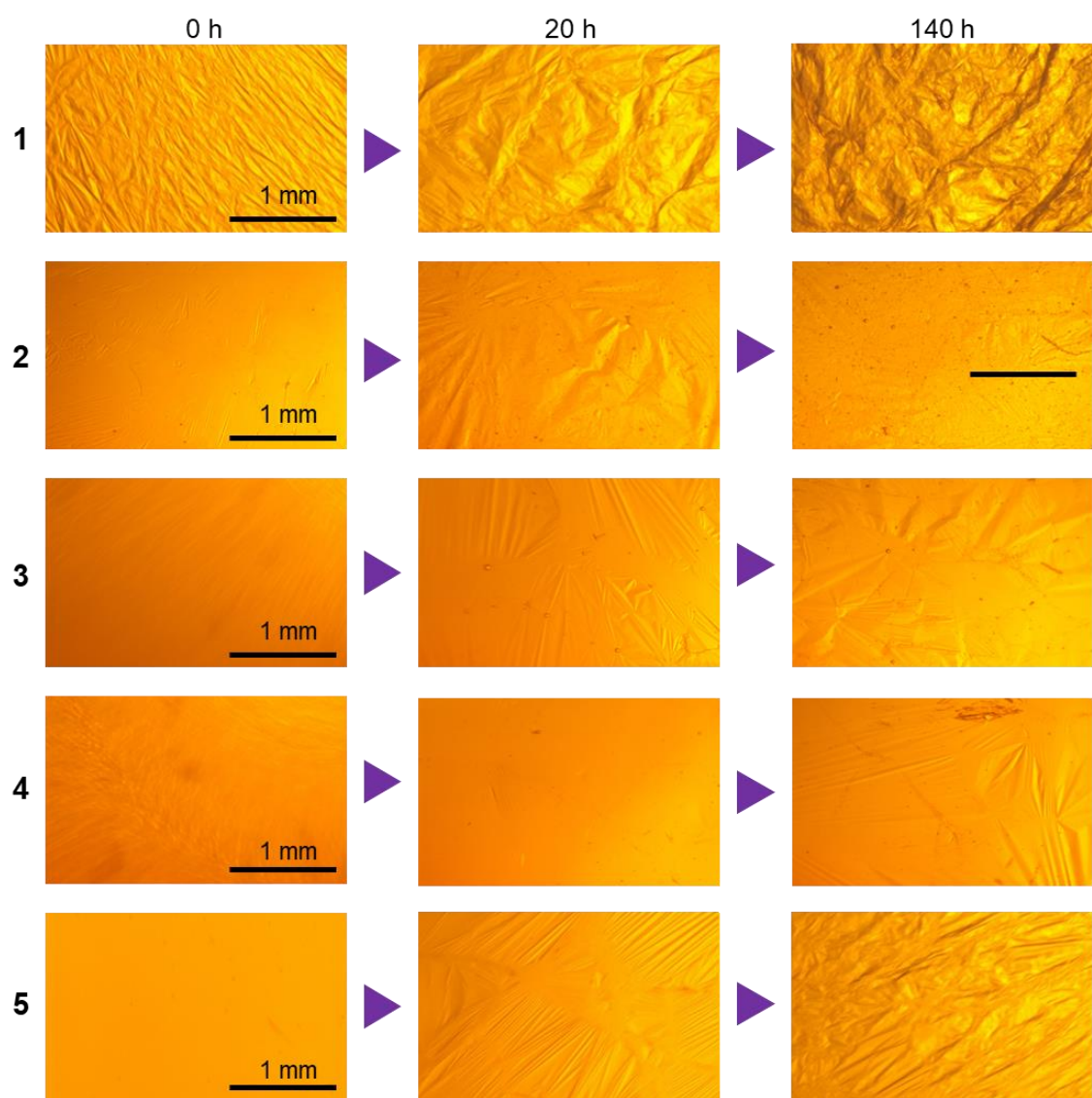


Fig. S18 Optical microscope images of the liquid-liquid interface of the SMM solution and $\text{Na}_2[\text{PdCl}_4]$ aq. The thickness of the film seemed to be increased over time. The images for **1** were taken from ref. 1.

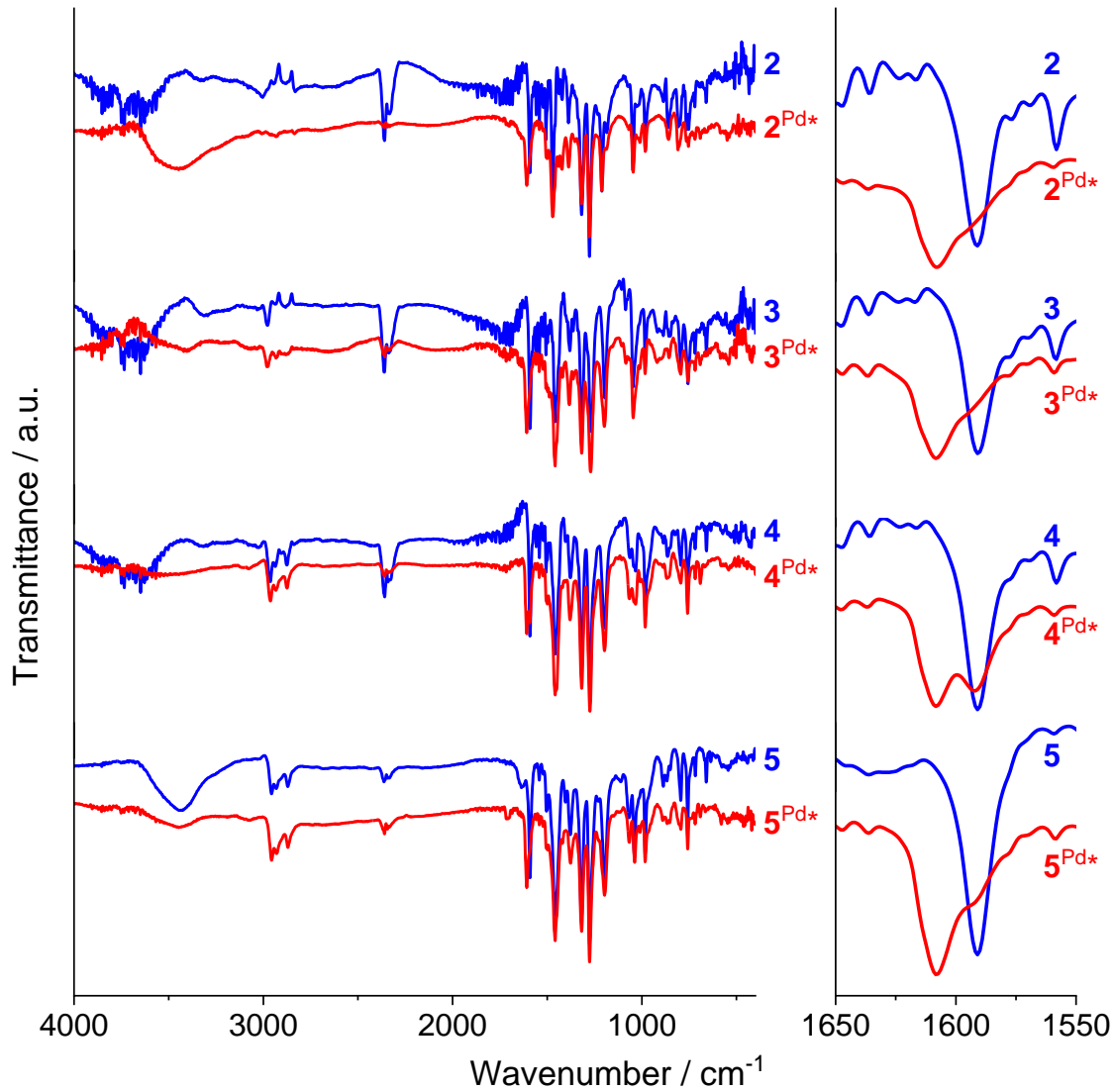


Fig. S19 IR spectra for **2-5** and $\mathbf{2}^{\text{Pd}*}$ - $\mathbf{5}^{\text{Pd}*}$ acquired using KBr pellet method. Enlarged spectra corresponding to the C=C stretching modes of Py units are shown for comparison.

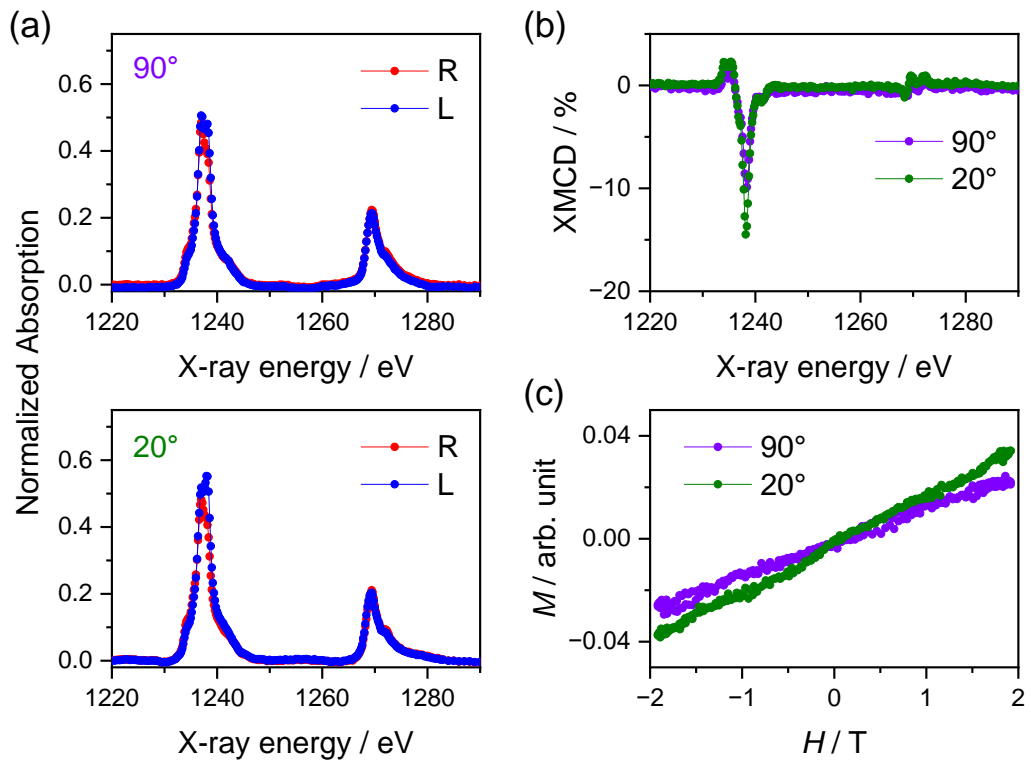


Fig. S20 (a) Normalized X-ray absorption, (b) XMCD spectra of $\mathbf{2}^{\text{aq}}$ deposited on the Si wafer measured at 11 K in the Tb $M_{4,5}$ region in an applied field of 1.9 T. Magnetic field was applied perpendicular (90°) and in-plane (20°) direction. (c) M vs. H curves derived from H-dependence of the XMCD intensity.

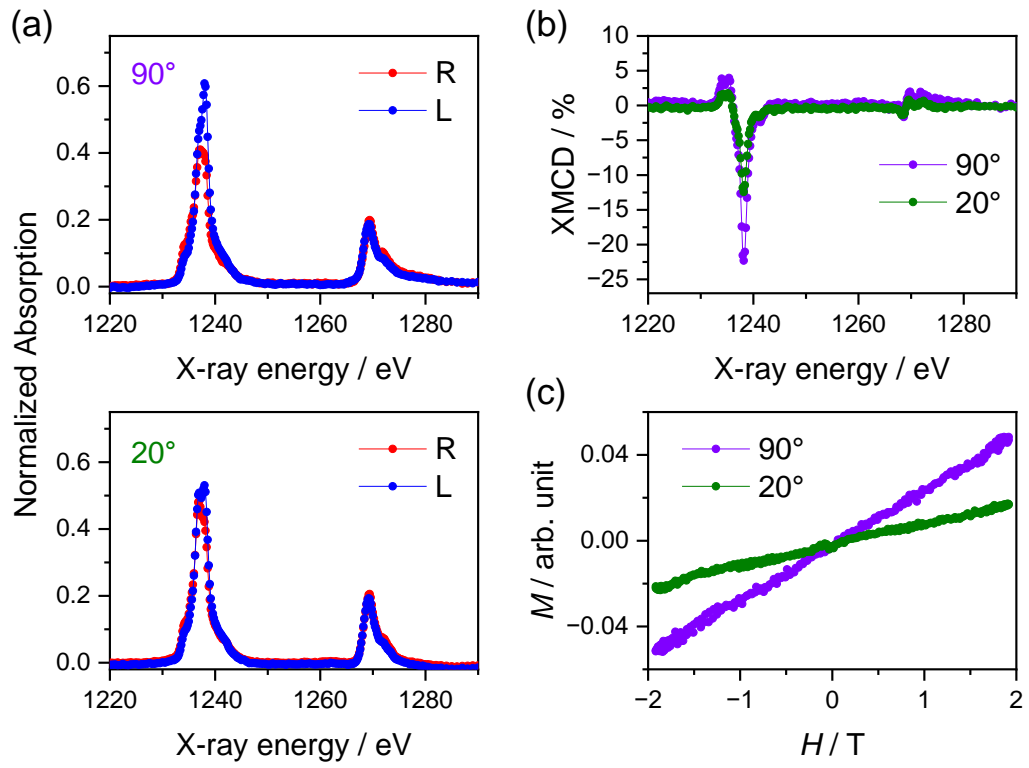


Fig. S21 (a) Normalized X-ray absorption, (b) XMCD spectra of $\mathbf{3}^{\text{aq}}$ deposited on the Si wafer measured at 11 K in the Tb $M_{4,5}$ region in an applied field of 1.9 T. Magnetic field was applied perpendicular (90°) and in-plane (20°) direction. (c) M vs. H curves derived from H-dependence of the XMCD intensity.

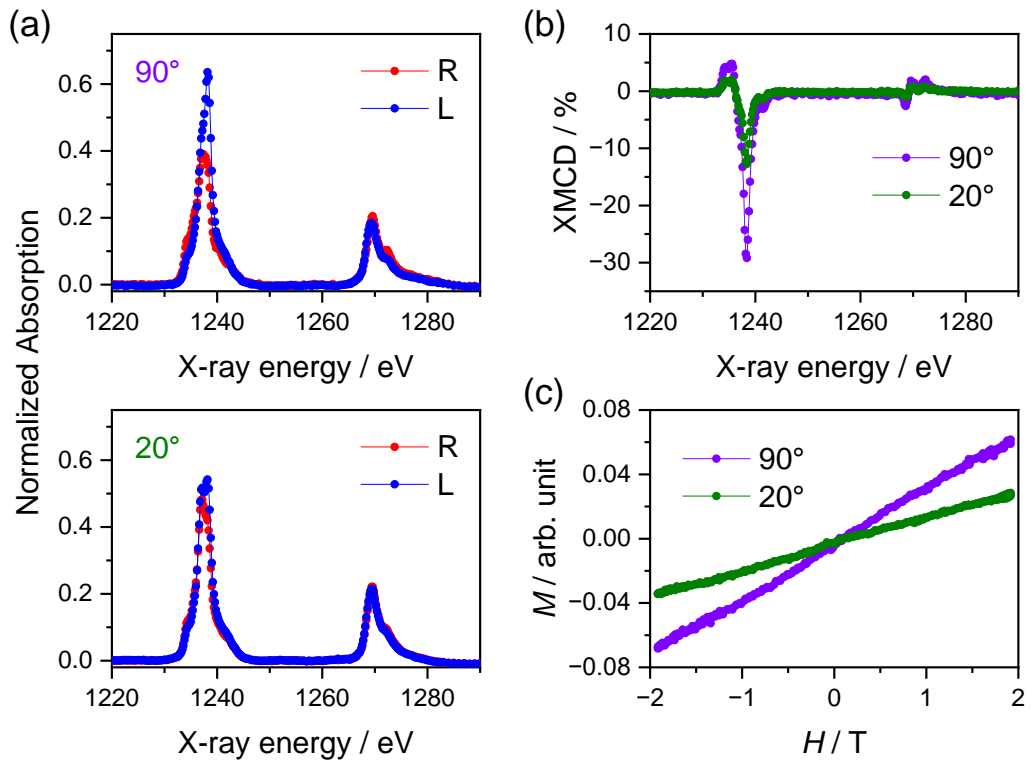


Fig. S22 (a) Normalized X-ray absorption, (b) XMCD spectra of **4^{aq}** deposited on the Si wafer measured at 11 K in the Tb $M_{4,5}$ region in an applied field of 1.9 T. Magnetic field was applied perpendicular (90°) and in-plane (20°) direction. (c) M vs. H curves derived from H-dependence of the XMCD intensity.

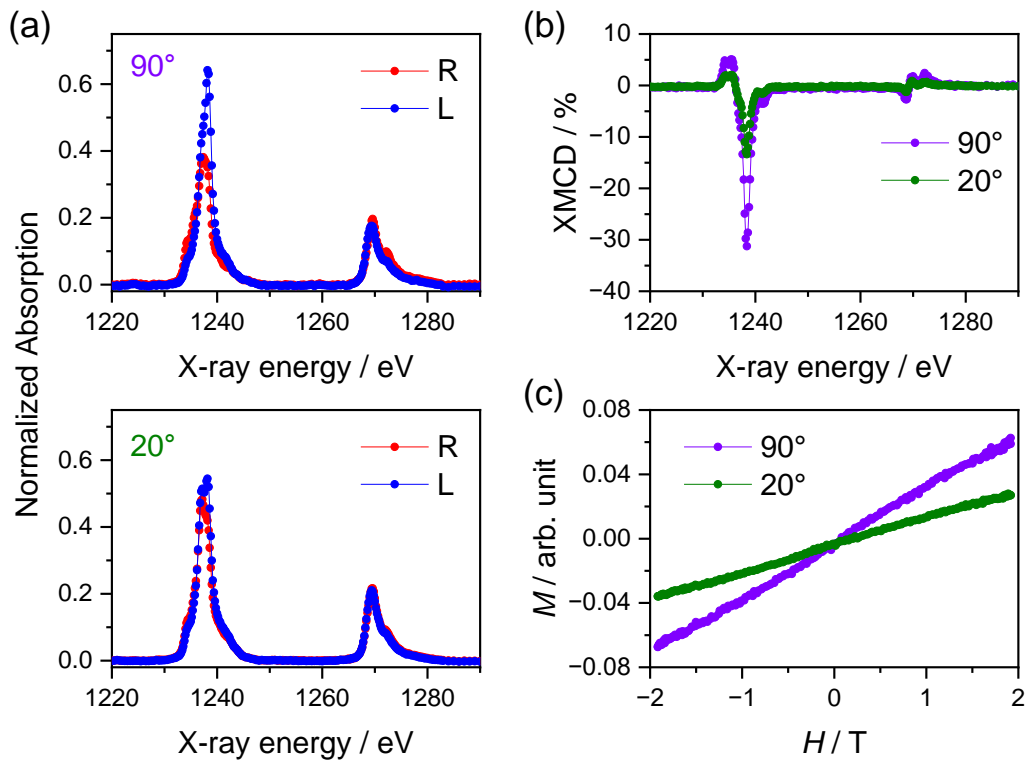


Fig. S23 (a) Normalized X-ray absorption, (b) XMCD spectra of 5^{aq} deposited on the Si wafer measured at 11 K in the Tb $M_{4,5}$ region in an applied field of 1.9 T. Magnetic field was applied perpendicular (90°) and in-plane (20°) direction. (c) M vs. H curves derived from H-dependence of the XMCD intensity.

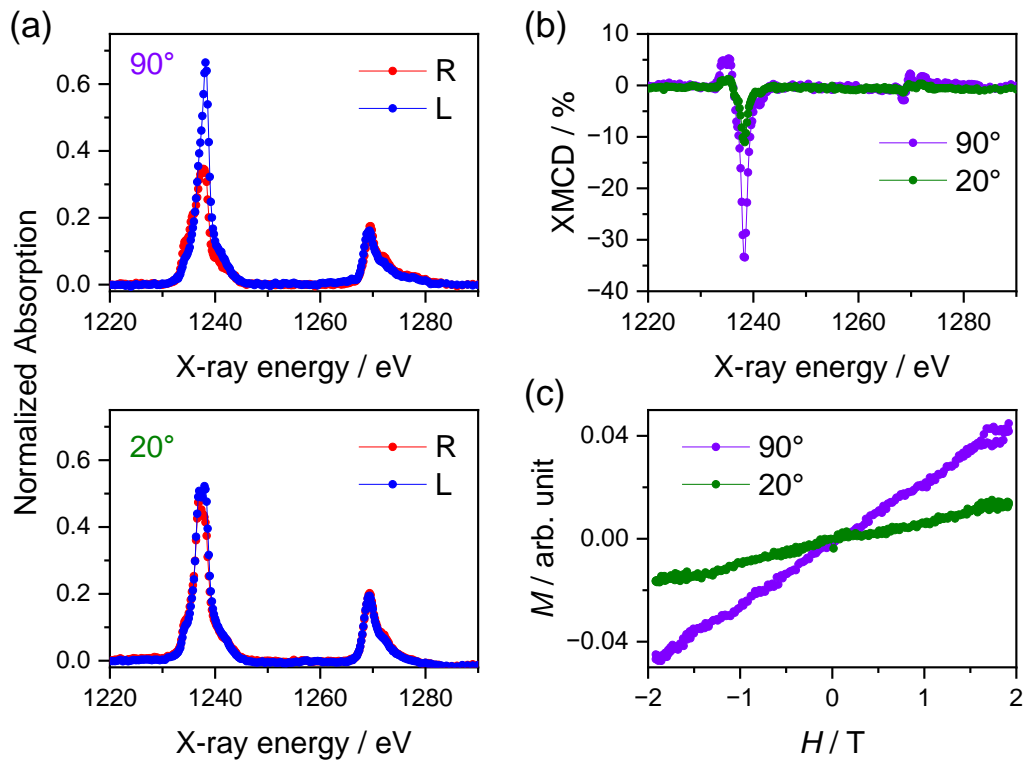


Fig. S24 (a) Normalized X-ray absorption, (b) XMCD spectra of 2^{Pd} deposited on the Si wafer measured at 11 K in the Tb $M_{4,5}$ region in an applied field of 1.9 T. Magnetic field was applied perpendicular (90°) and in-plane (20°) direction. (c) M vs. H curves derived from H-dependence of the XMCD intensity.

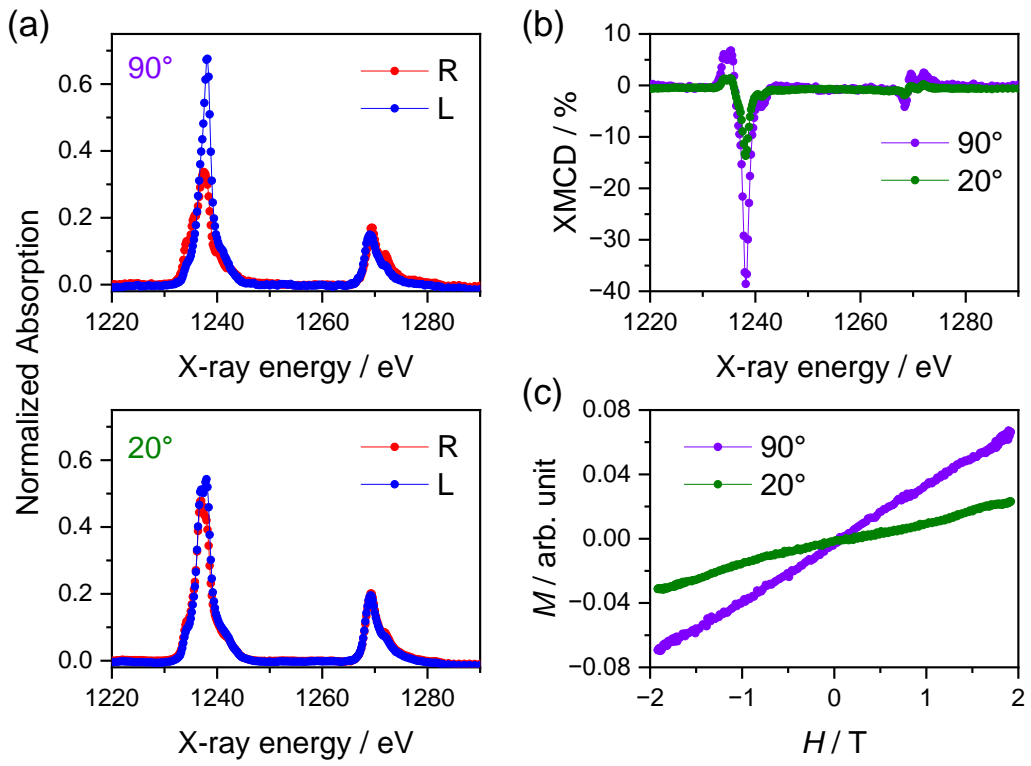


Fig. S25 (a) Normalized X-ray absorption, (b) XMCD spectra of ${}^3\text{P}_0$ deposited on the Si wafer measured at 11 K in the Tb $M_{4,5}$ region in an applied field of 1.9 T. Magnetic field was applied perpendicular (90°) and in-plane (20°) direction. (c) M vs. H curves derived from H-dependence of the XMCD intensity.

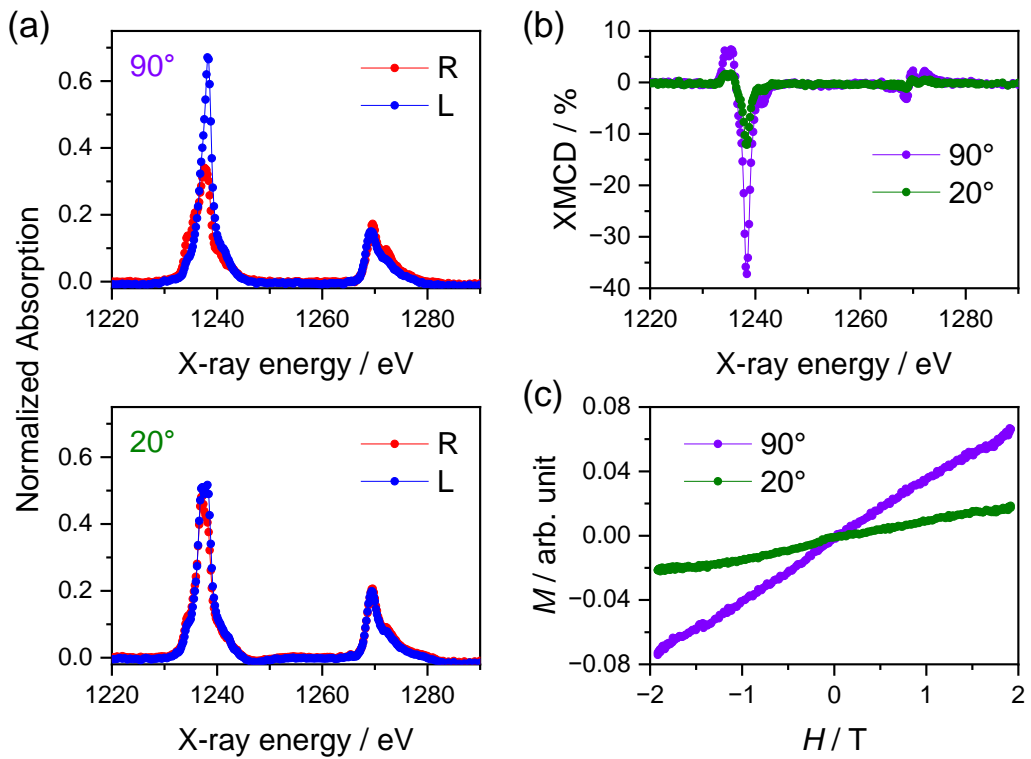


Fig. S26 (a) Normalized X-ray absorption, (b) XMCD spectra of $\mathbf{4}^{\text{Pd}}$ deposited on the Si wafer measured at 11 K in the Tb $M_{4,5}$ region in an applied field of 1.9 T. Magnetic field was applied perpendicular (90°) and in-plane (20°) direction. (c) M vs. H curves derived from H-dependence of the XMCD intensity.

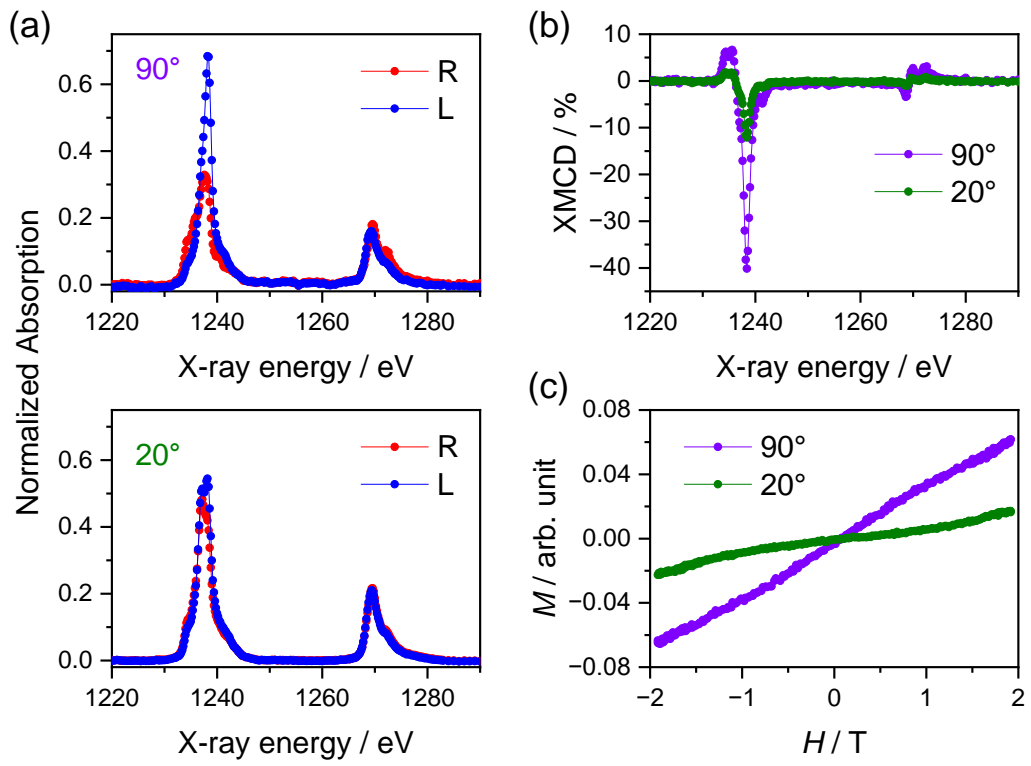


Fig. S27 (a) Normalized X-ray absorption, (b) XMCD spectra of ${}^5\text{Pd}$ deposited on the Si wafer measured at 11 K in the Tb $M_{4,5}$ region in an applied field of 1.9 T. Magnetic field was applied perpendicular (90°) and in-plane (20°) direction. (c) M vs. H curves derived from H-dependence of the XMCD intensity.

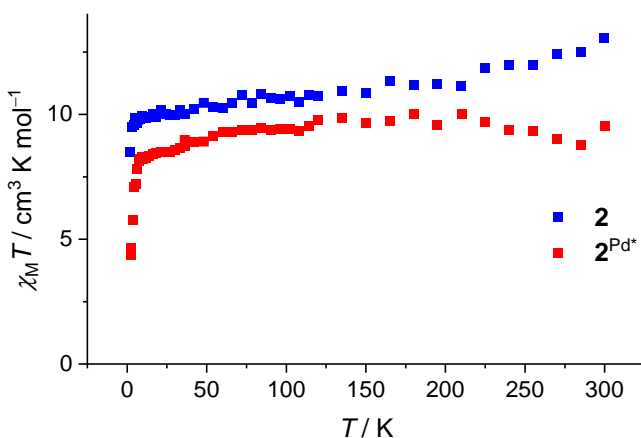


Fig. S28 $\chi_M T$ vs. T plots for **2** and **2**^{Pd*} at 1 kOe. $\chi_M T$ values were calculated based on the composition of C₈₀H₅₆N₁₆O₈Tb·2(CH₂Cl₂) for **2** and [C₈₀H₅₆N₁₆O₈TbPd][PdCl₄] (2+ densely-packed structure with a 2– counter anion) for **2**^{Pd*}.

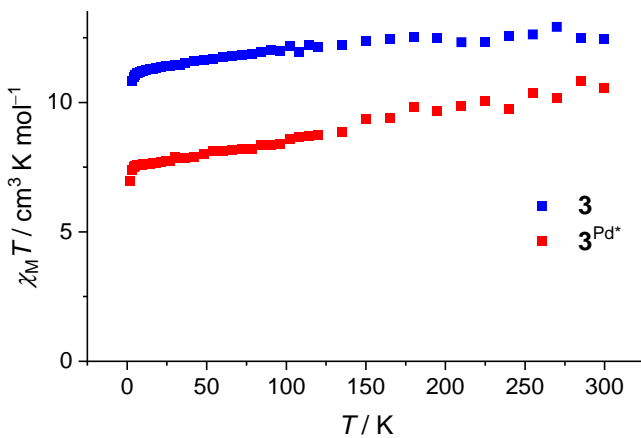


Fig. S29 $\chi_M T$ vs. T plots for **3** and **3**^{Pd*} at 1 kOe. $\chi_M T$ values were calculated based on the composition of C₈₈H₇₂N₁₆O₈Tb·3(CH₂Cl₂) for **3** and charge neutral C₈₈H₇₂N₁₆O₈TbPd₂Cl₄ for **3**^{Pd*}.

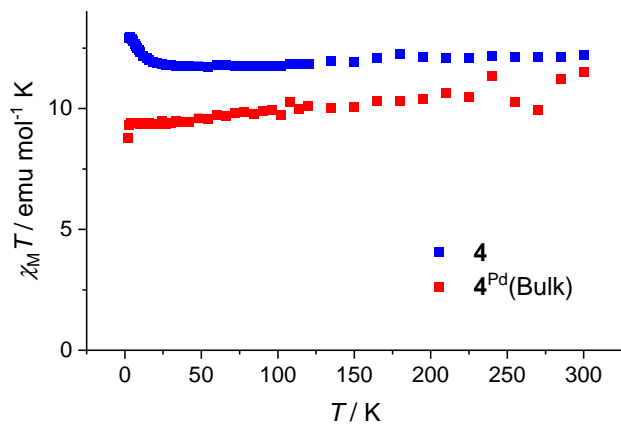


Fig. S30 $\chi_M T$ vs. T plots for **4** and **4^{Pd*}** at 1 kOe. $\chi_M T$ values were calculated based on the composition of $C_{96}H_{88}N_{16}O_8Tb \cdot 2(CH_2Cl_2) \cdot (C_6H_{14})$ for **4** and charge neutral $C_{96}H_{88}N_{16}O_8TbPd_2Cl_4$ for **4^{Pd*}**. **4** exhibited an increase in $\chi_M T$ values due to intermolecular ferromagnetic interactions.

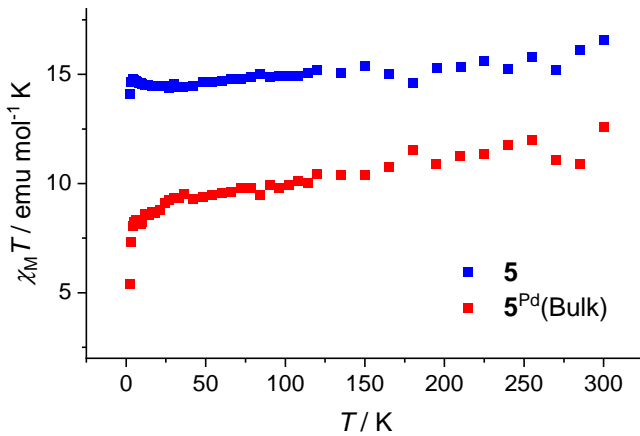


Fig. S31 $\chi_M T$ vs. T plots for **5** and **5^{Pd*}** at 1 kOe. $\chi_M T$ values were calculated based on the composition of $C_{104}H_{104}N_{16}O_8Tb \cdot 3(CH_2Cl_2)$ for **5** and charge neutral $C_{104}H_{104}N_{16}O_8TbPd_2Cl_4$ for **5^{Pd*}**.

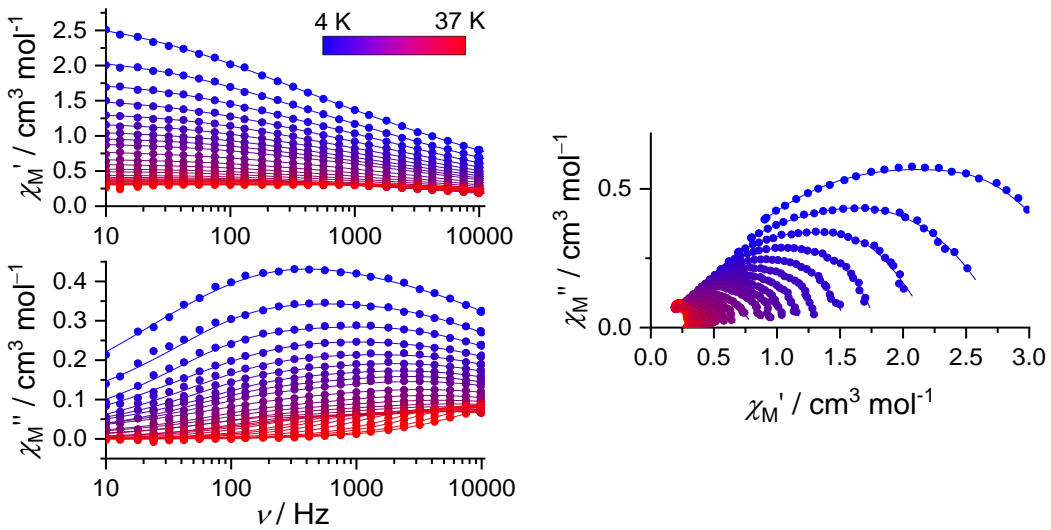


Fig. S32 AC magnetic susceptibility (left) and Argand plots (right) for **2** in a zero dc magnetic field. Solid curves represent a fit using extended Debye model.

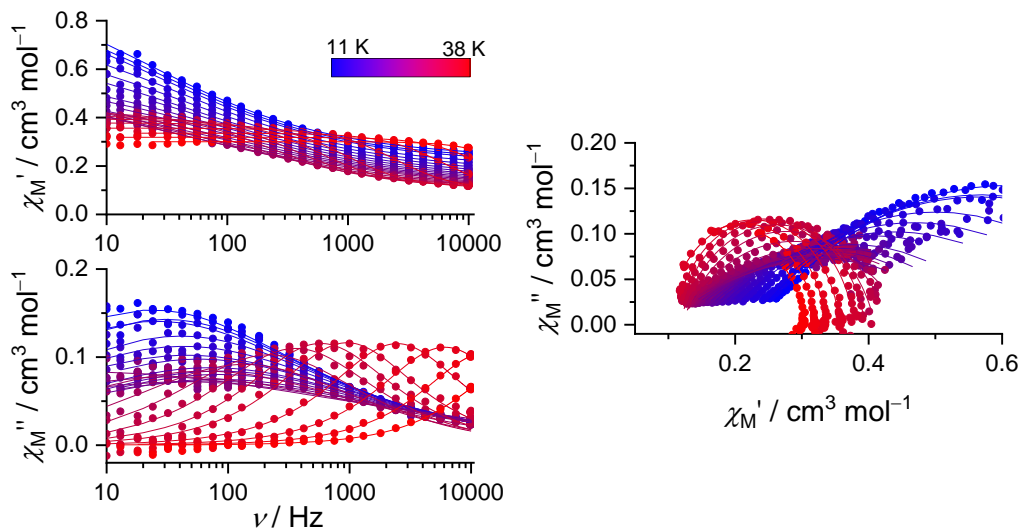


Fig. S33 AC magnetic susceptibility (left) and Argand plots (right) for **3** in a zero dc magnetic field. Solid curves represent a fit using generalized Debye model.

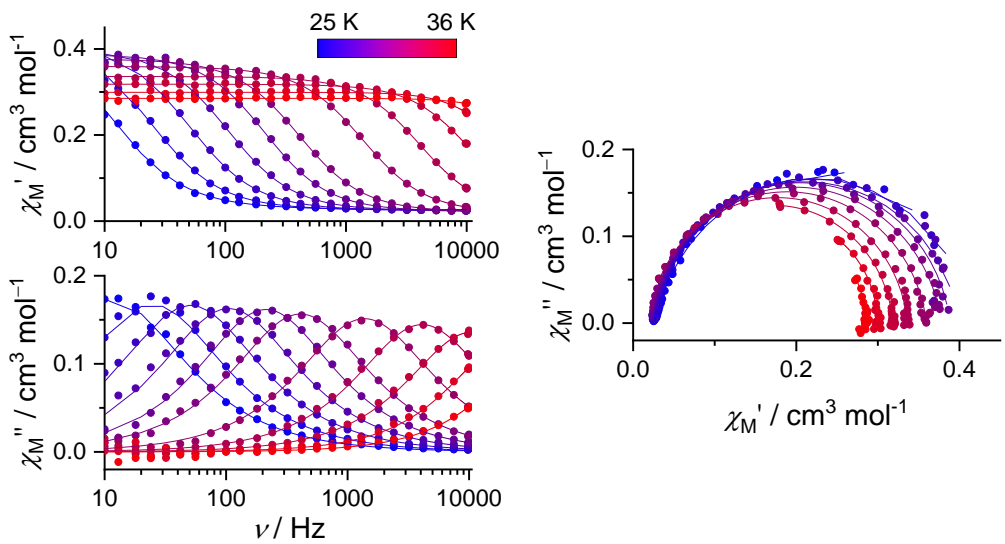


Fig. S34 AC magnetic susceptibility (left) and Argand plots (right) for **4** in a zero dc magnetic field. Solid curves represent a fit using generalized Debye model.

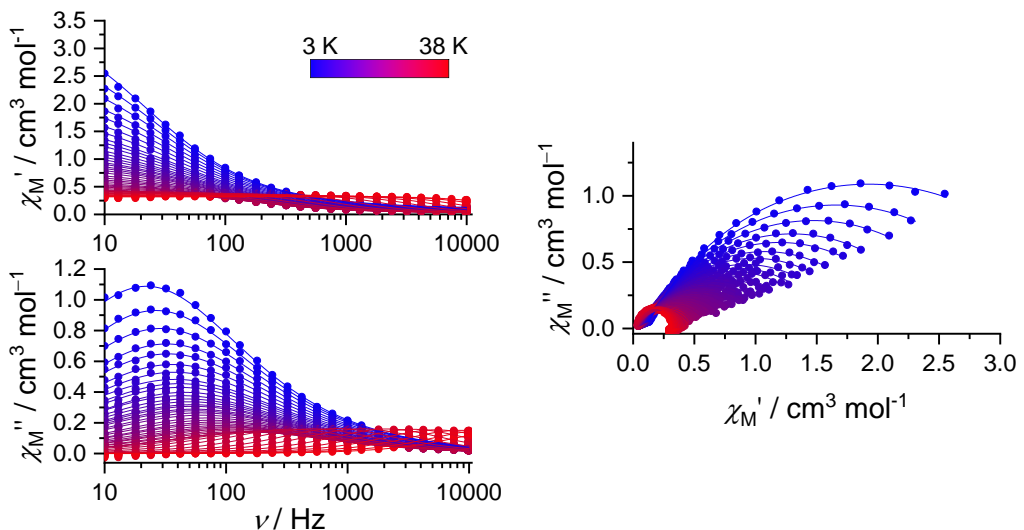


Fig. S35 AC magnetic susceptibility (left) and Argand plots (right) for **5** in a zero dc magnetic field. Solid curves represent a fit using generalized Debye model.

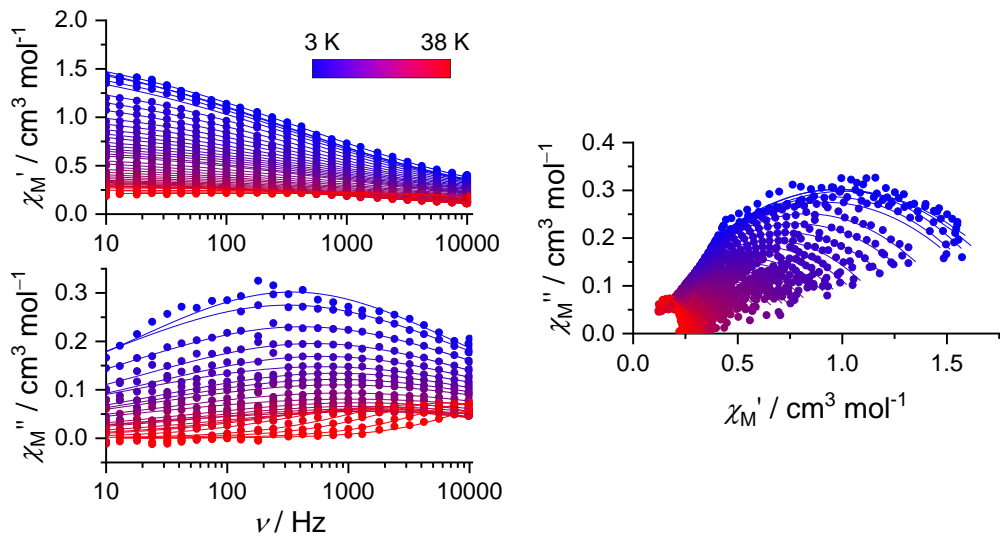


Fig. S36 AC magnetic susceptibility (left) and Argand plots (right) for $\mathbf{2}^{\text{Pd}*}$ in a zero dc magnetic field. Solid curves represent a fit using generalized Debye model.

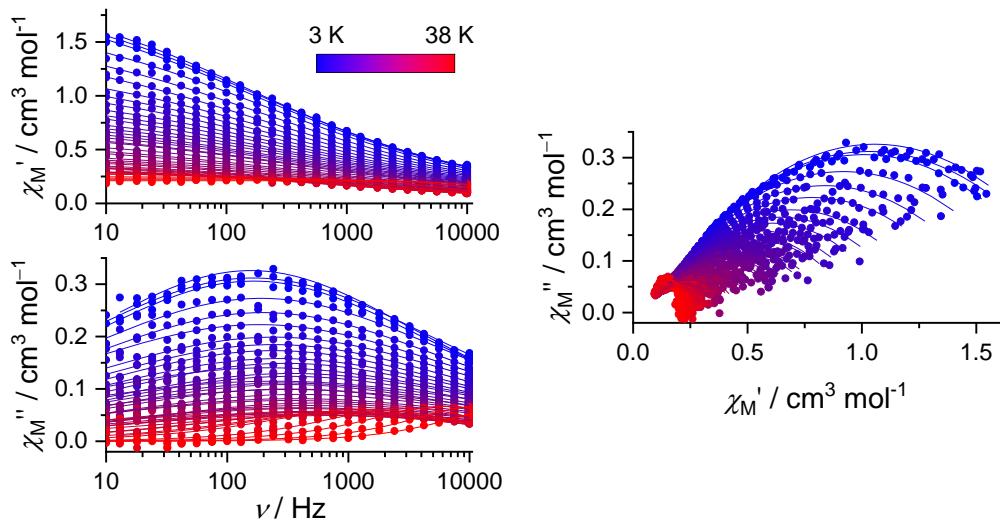


Fig. S37 AC magnetic susceptibility (left) and Argand plots (right) for $\mathbf{3}^{\text{Pd}*}$ in a zero dc magnetic field. Solid curves represent a fit using generalized Debye model.

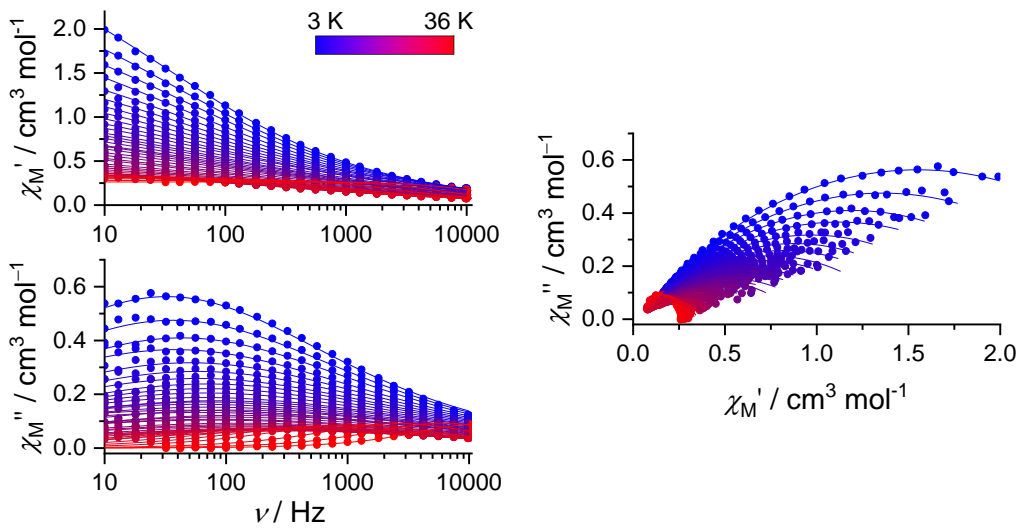


Fig. S38 AC magnetic susceptibility (left) and Argand plots (right) for **4^{Pd*}** in a zero dc magnetic field. Solid curves represent a fit using generalized Debye model.

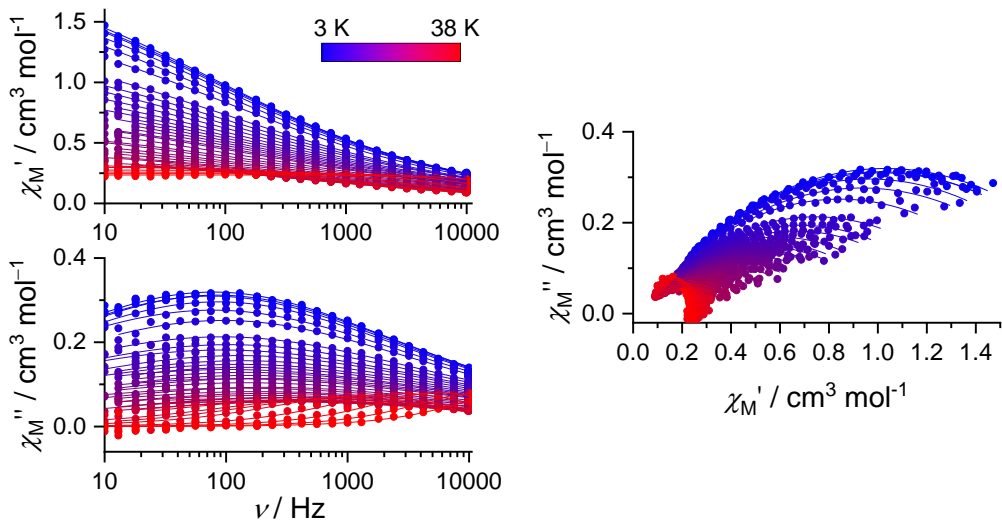


Fig. S39 AC magnetic susceptibility (left) and Argand plots (right) for **5^{Pd*}** in a zero dc magnetic field. Solid curves represent a fit using generalized Debye model.

Table S8. Parameters obtained by fitting the χ_M' and χ_M'' vs. ν plots of **2** at zero dc field using extended Debye model.

T / K	$\chi_T / \text{cm}^3 \text{ mol}^{-1}$	$\chi_S / \text{cm}^3 \text{ mol}^{-1}$	τ_1 / s	α_1	τ_2 / s	α_2	g
4.0	2.79(3)	0.21(2)	$8(4) \times 10^{-4}$	0.51(3)	$2(1) \times 10^{-5}$	0.5(2)	0.7(3)
5.0	2.23(4)	0.13(4)	$1.4(2) \times 10^{-4}$	0.1(2)	$1.2(4) \times 10^{-4}$	0.60(1)	0.07(6)
6.0	1.80(3)	0.17(5)	$1.5(2) \times 10^{-3}$	0.2(2)	$7(4) \times 10^{-5}$	0.54(5)	0.2(2)
7.0	1.56(2)	0.1(2)	$8(7) \times 10^{-4}$	0.4(2)	$3(5) \times 10^{-5}$	0.5(2)	0.4(7)
8.0	1.35(3)	0.1(1)	$9(5) \times 10^{-4}$	0.3(2)	$3(4) \times 10^{-5}$	0.5(2)	0.3(5)
9.0	1.22(1)	0.10(2)	$1.1(1) \times 10^{-3}$	0.1(2)	$5(1) \times 10^{-5}$	0.56(2)	0.08(5)
10.0	1.11(1)	0.08(2)	$9(1) \times 10^{-4}$	0.05(17)	$5(1) \times 10^{-5}$	0.58(1)	0.05(3)
11.0	0.99(2)	0.11(3)	$1.1(2) \times 10^{-3}$	0.1(3)	$5(2) \times 10^{-5}$	0.53(5)	0.1(1)
12.0	0.93(1)	0.08(2)	$1.0(2) \times 10^{-3}$	0	$4.9(9) \times 10^{-5}$	0.57(2)	0.04(3)
14.0	0.820(7)	0.046(9)	$10(1) \times 10^{-4}$	0	$4.6(5) \times 10^{-5}$	0.60(1)	0.02(2)
16.0	0.68(1)	0.08(3)	$10(2) \times 10^{-4}$	0.05(39)	$4(1) \times 10^{-5}$	0.54(5)	0.06(8)
18.0	0.62(1)	0.06(2)	$9(2) \times 10^{-4}$	0	$3.2(8) \times 10^{-5}$	0.55(3)	0.05(5)
20.0	0.54(1)	0.06(4)	$6(2) \times 10^{-4}$	0.2(4)	$2(1) \times 10^{-5}$	0.5(1)	0.1(2)
22.0	0.501(9)	0.08(3)	$1.1(2) \times 10^{-3}$	0.04(27)	$3.0(5) \times 10^{-5}$	0.50(8)	0.08(9)
24.0	0.440(4)	0.10(3)	$6(1) \times 10^{-4}$	0.07(20)	$2.3(5) \times 10^{-5}$	0.4(1)	0.2(2)
26.0	0.414(7)	0.08(6)	$5(2) \times 10^{-4}$	0.1(3)	$1.8(9) \times 10^{-5}$	0.4(3)	0.2(4)
28.0	0.393(4)	0.09(4)	$4(1) \times 10^{-4}$	0.1(2)	$2.1(8) \times 10^{-5}$	0.4(2)	0.2(3)
29.0	0.377(4)	0.10(4)	$4(1) \times 10^{-4}$	0	$2.4(7) \times 10^{-5}$	0.3(2)	0.2(3)
30.0	0.362(3)	0.11(5)	$2.3(5) \times 10^{-4}$	0	$1.8(7) \times 10^{-5}$	0.2(3)	0.3(4)
31.0	0.356(2)	0.11(4)	$1.7(9) \times 10^{-4}$	0.02(25)	$1.9(9) \times 10^{-5}$	0.2(3)	0.3(5)
32.0	0.348(1)	0.10(3)	$1.1(4) \times 10^{-4}$	0.03(19)	$1.6(7) \times 10^{-5}$	0.2(2)	0.3(4)
33.0	0.334(2)	0.12(6)	$8(5) \times 10^{-5}$	0	$1.3(5) \times 10^{-5}$	0.004(564)	0.4(7)
34.0	0.321(2)	0.1(4)	$0.4(10) \times 10^{-5}$	0	$9(9) \times 10^{-6}$	0	0.43
35.0	0.315(2)	0.1(6)	$3(9) \times 10^{-5}$	0	$0.6(10) \times 10^{-5}$	0	0.37
36.0	0.309(1)	0.12(1)	$1.3(1) \times 10^{-5}$	0.06(3)	0	0	1
37.0	0.3029(6)	0.10(1)	$8.1(9) \times 10^{-6}$	0.09(2)	0	0	1

* fixed at $0 \text{ cm}^3 \text{ mol}^{-1}$

Table S9. Parameters obtained by fitting the χ_M' and χ_M'' vs. ν plots of **3** at zero dc field using generalized Debye model.

T / K	$\chi_T / \text{cm}^3 \text{ mol}^{-1}$	$\chi_S / \text{cm}^3 \text{ mol}^{-1}$	τ / s	α
11.0	0.99(3)	0.231(5)	$6.7(9) \times 10^{-3}$	0.51(2)
11.5	0.92(2)	0.221(4)	$5.3(5) \times 10^{-3}$	0.51(1)
12.0	0.93(3)	0.209(5)	$6.1(8) \times 10^{-3}$	0.53(2)
13.0	0.81(2)	0.196(5)	$3.9(4) \times 10^{-3}$	0.51(2)
14.0	0.76(2)	0.176(5)	$3.7(4) \times 10^{-3}$	0.53(2)
15.0	0.72(2)	0.161(6)	$3.5(5) \times 10^{-3}$	0.55(2)
16.0	0.66(1)	0.154(4)	$2.8(2) \times 10^{-3}$	0.53(1)
17.0	0.61(2)	0.144(5)	$2.2(3) \times 10^{-3}$	0.54(2)
18.0	0.57(1)	0.138(4)	$2.0(2) \times 10^{-3}$	0.53(1)
19.0	0.55(1)	0.130(4)	$1.9(2) \times 10^{-3}$	0.54(1)
20.0	0.54(2)	0.119(7)	$2.0(3) \times 10^{-3}$	0.56(2)
21.0	0.54(2)	0.110(6)	$2.3(3) \times 10^{-3}$	0.58(2)
26.0	0.458(9)	0.117(5)	$1.17(9) \times 10^{-3}$	0.37(2)
27.0	0.432(5)	0.120(3)	$7.3(3) \times 10^{-4}$	0.26(2)
28.0	0.409(4)	0.117(4)	$4.4(2) \times 10^{-4}$	0.18(2)
29.0	0.395(2)	0.114(3)	$2.75(7) \times 10^{-4}$	0.12(1)
30.0	0.378(2)	0.109(3)	$1.67(4) \times 10^{-4}$	0.09(1)
32.0	0.357(2)	0.098(4)	$6.5(2) \times 10^{-5}$	0.07(1)
34.0	0.3356(7)	0.091(4)	$2.62(5) \times 10^{-5}$	0.06(1)
36.0	0.3187(5)	0.095(7)	$1.20(5) \times 10^{-5}$	0.04(1)
38.0	0.300(1)	0.12(4)	$7(2) \times 10^{-6}$	0

* fixed at $0 \text{ cm}^3 \text{ mol}^{-1}$

Table S10. Parameters obtained by fitting the χ_M' and χ_M'' vs. ν plots of **4** at zero dc field using generalized Debye model.

T / K	χ_T / $\text{cm}^3 \text{ mol}^{-1}$	χ_S / $\text{cm}^3 \text{ mol}^{-1}$	τ / s	α
25.0	0.460(8)	0.0263(7)	$1.44(5) \times 10^{-2}$	0.51(2)
26.0	0.425(5)	0.0250(9)	$6.5(1) \times 10^{-3}$	0.51(1)
27.0	0.415(3)	0.0239(9)	$3.14(4) \times 10^{-3}$	0.53(2)
28.0	0.399(3)	0.023(1)	$1.51(2) \times 10^{-3}$	0.51(2)
29.0	0.389(2)	0.022(1)	$7.48(9) \times 10^{-4}$	0.53(2)
30.0	0.378(1)	0.020(1)	$3.89(3) \times 10^{-4}$	0.55(2)
32.0	0.3595(8)	0.018(1)	$1.16(1) \times 10^{-4}$	0.53(1)
34.0	0.336(1)	0.018(3)	$3.88(6) \times 10^{-5}$	0.54(2)
36.0	0.318(1)	0.02(1)	$1.53(8) \times 10^{-5}$	0.53(1)
38.0	0.299(1)	0.06(3)	$8(1) \times 10^{-6}$	0.54(1)

* fixed at 0 $\text{cm}^3 \text{ mol}^{-1}$

Table S11. Parameters obtained by fitting the χ_M' and χ_M'' vs. v plots of **5** at zero dc field using generalized Debye model.

T / K	χ_T / $\text{cm}^3 \text{ mol}^{-1}$	χ_S / $\text{cm}^3 \text{ mol}^{-1}$	τ / s	α
3.0	3.30(2)	0.090(4)	$7.2(1) \times 10^{-3}$	0.315(4)
3.5	2.84(2)	0.083(3)	$6.06(8) \times 10^{-3}$	0.317(3)
4.0	2.52(1)	0.075(2)	$5.51(7) \times 10^{-3}$	0.326(3)
4.5	2.21(1)	0.070(2)	$4.91(6) \times 10^{-3}$	0.326(3)
5.0	2.04(1)	0.065(2)	$4.77(6) \times 10^{-3}$	0.332(3)
5.5	1.83(1)	0.061(2)	$4.40(7) \times 10^{-3}$	0.335(4)
6.0	1.68(1)	0.059(2)	$4.23(7) \times 10^{-3}$	0.337(4)
6.5	1.56(2)	0.053(5)	$4.2(2) \times 10^{-3}$	0.35(1)
7.0	1.444(9)	0.055(2)	$3.86(7) \times 10^{-3}$	0.334(5)
7.5	1.373(9)	0.052(2)	$3.83(7) \times 10^{-3}$	0.337(5)
8.0	1.251(8)	0.053(2)	$3.48(5) \times 10^{-3}$	0.326(4)
8.5	1.215(8)	0.048(2)	$3.66(6) \times 10^{-3}$	0.343(4)
9.0	1.125(8)	0.049(2)	$3.35(6) \times 10^{-3}$	0.331(5)
9.5	0.359(4)	0.047(2)	$3.19(6) \times 10^{-3}$	0.26(2)
10.0	0.998(7)	0.046(2)	$3.02(6) \times 10^{-3}$	0.324(6)
10.5	0.960(4)	0.046(1)	$2.97(4) \times 10^{-3}$	0.320(4)
11.0	0.918(8)	0.042(2)	$2.91(7) \times 10^{-3}$	0.331(7)
11.5	0.878(7)	0.042(2)	$2.85(6) \times 10^{-3}$	0.326(6)
12.0	0.821(7)	0.0043(2)	$2.60(5) \times 10^{-3}$	0.313(7)
13.0	0.776(5)	0.040(2)	$2.54(5) \times 10^{-3}$	0.315(6)
14.0	0.703(6)	0.039(2)	$2.25(5) \times 10^{-3}$	0.300(7)
15.0	0.662(5)	0.037(2)	$2.15(4) \times 10^{-3}$	0.303(6)
16.0	0.614(5)	0.037(2)	$1.93(4) \times 10^{-3}$	0.288(8)
17.0	0.589(6)	0.034(2)	$1.89(5) \times 10^{-3}$	0.30(1)
18.0	0.544(6)	0.034(3)	$1.74(5) \times 10^{-3}$	0.29(1)
19.0	0.514(6)	0.032(3)	$1.57(5) \times 10^{-3}$	0.28(1)
20.0	0.491(3)	0.032(2)	$1.45(3) \times 10^{-3}$	0.272(7)
21.0	0.472(4)	0.030(2)	$1.41(3) \times 10^{-3}$	0.280(8)
22.0	0.439(2)	0.031(1)	$1.23(2) \times 10^{-3}$	0.258(6)
23.0	0.419(3)	0.028(2)	$1.17(3) \times 10^{-3}$	0.27(1)
24.0	0.388(6)	0.029(3)	$9.9(4) \times 10^{-4}$	0.24(2)
25.0	0.392(3)	0.028(2)	$1.00(2) \times 10^{-3}$	0.249(9)
26.0	0.394(3)	0.027(2)	$9.5(2) \times 10^{-4}$	0.24(1)

27.0	0.385(4)	0.028(3)	$8.1(2) \times 10^{-4}$	0.22(1)
28.0	0.377(3)	0.030(2)	$6.4(1) \times 10^{-4}$	0.17(1)
29.0	0.368(3)	0.031(3)	$4.6(1) \times 10^{-4}$	0.12(1)
30.0	0.354(2)	0.031(3)	$3.06(7) \times 10^{-4}$	0.08(1)
31.0	0.341(2)	0.031(3)	$1.95(5) \times 10^{-4}$	0.05(1)
32.0	0.333(2)	0.027(3)	$1.22(2) \times 10^{-4}$	0.05(1)
33.0	0.321(2)	0.028(4)	$7.5(2) \times 10^{-5}$	0.03(1)
34.0	0.310(2)	0.026(6)	$4.6(1) \times 10^{-5}$	0.01(2)
35.0	0.304(1)	0.028(6)	$2.99(9) \times 10^{-5}$	0.01(2)
36.0	0.295(2)	0.03(1)	$1.9(1) \times 10^{-5}$	0.001(28)
37.0	0.287(2)	0.02(2)	$1.2(1) \times 10^{-5}$	0
38.0	0.280(2)	0.03(4)	$8.7(2) \times 10^{-6}$	0

* fixed at $0 \text{ cm}^3 \text{ mol}^{-1}$

Table S12. Parameters obtained by fitting the χ_M' and χ_M'' vs. v plots of $\text{2}^{\text{Pd}*}$ at zero dc field using generalized Debye model.

T / K	$\chi_T / \text{cm}^3 \text{ mol}^{-1}$	$\chi_S / \text{cm}^3 \text{ mol}^{-1}$	τ / s	α
4.0	1.88(3)	0.06(3)	$4.6(3) \times 10^{-4}$	0.5904(2)
5.0	1.83(6)	0.02(2)	$5.0(6) \times 10^{-4}$	0.6246(4)
6.0	1.54(1)	0.01(1)	$3.9(1) \times 10^{-4}$	0.62784(3)
7.0	1.29(2)	0.04(2)	$3.1(2) \times 10^{-4}$	0.6151
8.0	1.13(1)	0.03(2)	$2.6(1) \times 10^{-4}$	0.61817(4)
9.0	1.06(2)	0*	$2.7(2) \times 10^{-4}$	0.65469(4)
10.0	0.90(1)	0.03(2)	$2.1(2) \times 10^{-4}$	0.61622(6)
11.0	0.83(1)	0.03(2)	$2.0(2) \times 10^{-4}$	0.62283(4)
12.0	0.78(1)	0.02(2)	$1.9(2) \times 10^{-4}$	0.63991(3)
14.0	0.66(1)	0.02(2)	$1.7(2) \times 10^{-4}$	0.6398
16.0	0.60(2)	0*	$1.5(3) \times 10^{-4}$	0.66695(4)
18.0	0.492(9)	0.04(2)	$1.3(2) \times 10^{-4}$	0.60994(3)
20.0	0.446(8)	0.04(2)	$1.2(2) \times 10^{-4}$	0.59834(3)
22.0	0.411(9)	0.04(2)	$1.2(2) \times 10^{-4}$	0.59633(3)
24.0	0.41(1)	0*	$1.0(3) \times 10^{-4}$	0.66344(4)
26.0	0.346(6)	0.05(1)	$1.2(2) \times 10^{-4}$	0.53854(3)
28.0	0.325(6)	0.07(1)	$1.2(2) \times 10^{-4}$	0.45977(8)
29.0	0.319(4)	0.067(9)	$1.0(1) \times 10^{-4}$	0.42708(4)
30.0	0.300(3)	0.080(8)	$8.6(8) \times 10^{-5}$	0.32773(4)
32.0	0.271(3)	0.08(1)	$4.5(5) \times 10^{-5}$	0.20523(9)
34.0	0.264(2)	0.08(1)	$2.6(2) \times 10^{-5}$	0.1633
36.0	0.248(1)	0.08(1)	$1.5(1) \times 10^{-5}$	0.08479(1)
38.0	0.235(1)	0.09(3)	$8(2) \times 10^{-6}$	0.03088(2)

* fixed at $0 \text{ cm}^3 \text{ mol}^{-1}$

Table S13. Parameters obtained by fitting the χ_M' and χ_M'' vs. v plots of $\mathbf{3}^{\text{pd}*}$ at zero dc field using generalized Debye model.

T / K	$\chi_T / \text{cm}^3 \text{ mol}^{-1}$	$\chi_S / \text{cm}^3 \text{ mol}^{-1}$	τ / s	α
3.0	1.94(2)	0.08(1)	$9.7(3) \times 10^{-4}$	0.59704(5)
3.5	2.02(2)	0.09(1)	$1.02(5) \times 10^{-3}$	0.58574(9)
4.0	2.02(3)	0.05(2)	$9.7(6) \times 10^{-4}$	0.60858(1)
4.5	1.80(3)	0.04(2)	$8.4(6) \times 10^{-4}$	0.6179(1)
5.0	1.64(4)	0.04(3)	$8.1(8) \times 10^{-4}$	0.6204(2)
5.5	1.54(2)	0.02(1)	$8.6(4) \times 10^{-4}$	0.63788(4)
6.0	1.36(3)	0.02(2)	$6.6(5) \times 10^{-4}$	0.63092(9)
6.5	1.25(2)	0.04(2)	$6.5(5) \times 10^{-4}$	0.62406(8)
7.0	1.16(3)	0.05(2)	$6.6(5) \times 10^{-4}$	0.61757(9)
7.5	1.08(2)	0.04(2)	$5.8(4) \times 10^{-4}$	0.62565(6)
8.0	0.99(2)	0.05(2)	$5.2(5) \times 10^{-4}$	0.6085(1)
8.5	1.02(3)	0.02(2)	$7.2(7) \times 10^{-4}$	0.65079(6)
9.0	0.89(2)	0.03(2)	$4.7(5) \times 10^{-4}$	0.62874(7)
9.5	0.84(2)	0.05(2)	$4.8(4) \times 10^{-4}$	0.61598(7)
10.0	0.89(3)	0*	$6.5(9) \times 10^{-4}$	0.67815(7)
10.5	0.79(2)	0.04(2)	$5.3(5) \times 10^{-4}$	0.63161(5)
11.0	0.73(2)	0.06(2)	$5.0(6) \times 10^{-4}$	0.6038(1)
11.5	0.73(3)	0.02(3)	$5.0(9) \times 10^{-4}$	0.6527(1)
12.0	0.68(2)	0.06(2)	$5.0(6) \times 10^{-4}$	0.60695(7)
13.0	0.62(2)	0.04(2)	$3.9(5) \times 10^{-4}$	0.61434(6)
14.0	0.59(2)	0.03(2)	$4.4(7) \times 10^{-4}$	0.64078(7)
15.0	0.58(1)	0.03(1)	$4.8(5) \times 10^{-4}$	0.64574(2)
16.0	0.48(2)	0.06(2)	$3.2(5) \times 10^{-4}$	0.5687(1)
17.0	0.47(2)	0.05(2)	$3.4(7) \times 10^{-4}$	0.5979(1)
18.0	0.47(2)	0.03(2)	$4.0(7) \times 10^{-4}$	0.63375(6)
19.0	0.44(1)	0.05(1)	$4.0(4) \times 10^{-4}$	0.60281(3)
20.0	0.41(2)	0.04(2)	$3.1(7) \times 10^{-4}$	0.6196
21.0	0.38(2)	0.04(3)	$3.1(9) \times 10^{-4}$	0.5973(1)
22.0	0.37(2)	0.05(2)	$3.3(7) \times 10^{-4}$	0.58586(9)
23.0	0.44(3)	0*	$6.3(2) \times 10^{-4}$	0.70984(4)
24.0	0.31(1)	0.06(2)	$2.3(5) \times 10^{-4}$	0.4885(1)
25.0	0.36(1)	0.03(1)	$3.5(4) \times 10^{-4}$	0.61483(2)
26.0	0.33(2)	0.03(2)	$2.3(6) \times 10^{-4}$	0.59813(9)

27.0	0.302(8)	0.06(1)	$2.3(4) \times 10^{-4}$	0.47653(8)
28.0	0.284(7)	0.06(1)	$1.7(3) \times 10^{-4}$	0.4097(1)
29.0	0.279(5)	0.058(9)	$1.4(2) \times 10^{-4}$	0.39286(5)
30.0	0.275(4)	0.063(8)	$1.2(1) \times 10^{-4}$	0.33697(7)
32.0	0.247(3)	0.065(9)	$5.4(6) \times 10^{-5}$	0.22364(7)
34.0	0.235(2)	0.06(1)	$2.6(3) \times 10^{-5}$	0.18009(3)
36.0	0.221(2)	0.07(3)	$1.4(4) \times 10^{-5}$	0.09616(8)
38.0	0.211(2)	0.08(5)	$8(4) \times 10^{-6}$	0.07271(5)

* fixed at 0 cm³ mol⁻¹

Table S14. Parameters obtained by fitting the χ_M' and χ_M'' vs. v plots of **4^{Pd*}** at zero dc field using generalized Debye model.

T / K	χ_T / cm ³ mol ⁻¹	χ_S / cm ³ mol ⁻¹	τ / s	α
3.0	3.09(4)	0.008(8)	$4.9(2) \times 10^{-3}$	0.555(5)
3.5	2.72(4)	0*	$4.4(3) \times 10^{-3}$	0.572(7)
4.0	2.39(3)	0*	$3.7(2) \times 10^{-3}$	0.579(5)
4.5	2.24(5)	0*	$4.2(4) \times 10^{-3}$	0.60(1)
5.0	1.94(4)	0*	$3.1(3) \times 10^{-3}$	0.60(1)
5.5	1.76(4)	0*	$2.8(2) \times 10^{-3}$	0.60(1)
6.0	1.65(3)	0*	$2.7(2) \times 10^{-3}$	0.61(1)
6.5	1.49(3)	0*	$2.3(2) \times 10^{-3}$	0.607(9)
7.0	1.42(3)	0*	$2.3(2) \times 10^{-3}$	0.61(1)
7.5	1.34(3)	0*	$2.3(2) \times 10^{-3}$	0.62(1)
8.0	1.29(5)	0*	$2.5(4) \times 10^{-3}$	0.64(2)
8.5	1.16(3)	0*	$1.9(2) \times 10^{-3}$	0.62(1)
9.0	1.16(3)	0*	$2.4(3) \times 10^{-3}$	0.63(1)
9.5	1.14(3)	0*	$2.7(3) \times 10^{-3}$	0.65(1)
10.0	1.06(4)	0*	$2.3(4) \times 10^{-3}$	0.64(2)
10.5	0.93(3)	0.003(12)	$1.5(2) \times 10^{-3}$	0.62(1)
11.0	1.04(6)	0*	$3.3(8) \times 10^{-3}$	0.66(2)
11.5	0.97(4)	0*	$2.7(5) \times 10^{-3}$	0.66(2)
12.0	0.81(3)	0.004(15)	$1.3(2) \times 10^{-3}$	0.63(2)
13.0	0.81(3)	0*	$1.7(3) \times 10^{-3}$	0.65(2)
14.0	0.77(4)	0*	$1.9(4) \times 10^{-3}$	0.66(2)
15.0	0.75(2)	0*	$2.1(2) \times 10^{-3}$	0.66(1)
16.0	0.64(2)	0.003(13)	$1.3(2) \times 10^{-3}$	0.64(2)
17.0	0.60(2)	0.006(10)	$1.2(1) \times 10^{-3}$	0.64(2)
18.0	0.58(2)	0*	$1.2(2) \times 10^{-3}$	0.65(2)
19.0	0.51(2)	0.02(1)	$9(1) \times 10^{-4}$	0.61(2)
20.0	0.48(2)	0.02(1)	$7.5(9) \times 10^{-4}$	0.60(2)
21.0	0.44(1)	0.027(9)	$6.6(7) \times 10^{-4}$	0.58(2)
22.0	0.47(2)	0.01(1)	$9.4(1) \times 10^{-4}$	0.63(2)
23.0	0.42(1)	0.02(9)	$6.8(8) \times 10^{-4}$	0.60(2)
24.0	0.37(1)	0.029(9)	$4.4(5) \times 10^{-4}$	0.54(3)
25.0	0.43(1)	0.020(7)	$8.2(8) \times 10^{-4}$	0.59(2)
26.0	0.39(1)	0.031(6)	$5.6(5) \times 10^{-4}$	0.52(2)

27.0	0.377(6)	0.038(4)	$4.4(2) \times 10^{-4}$	0.47(2)
28.0	0.353(4)	0.044(4)	$3.1(1) \times 10^{-4}$	0.40(1)
29.0	0.338(3)	0.045(3)	$2.09(7) \times 10^{-4}$	0.35(1)
30.0	0.322(2)	0.048(3)	$1.39(4) \times 10^{-4}$	0.29(1)
32.0	0.301(1)	0.044(3)	$6.0(2) \times 10^{-5}$	0.22(1)
34.0	0.281(1)	0.041(4)	$2.61(8) \times 10^{-5}$	0.16(1)
36.0	0.2632(5)	0.053(6)	$1.30(6) \times 10^{-5}$	0.10(1)

* fixed at 0 cm³ mol⁻¹

Table S15. Parameters obtained by fitting the χ_M' and χ_M'' vs. v plots of **5^{Pd*}** at zero dc field using generalized Debye model.

T / K	χ_T / cm ³ mol ⁻¹	χ_S / cm ³ mol ⁻¹	τ / s	α
3.0	2.34(3)	0.005(12)	$2.0(1) \times 10^{-3}$	0.616(6)
3.5	2.29(3)	0*	$1.9(1) \times 10^{-3}$	0.617(7)
4.0	2.30(3)	0*	$2.1(1) \times 10^{-3}$	0.622(6)
4.5	2.19(3)	1.4×10^{-4}	$1.9(1) \times 10^{-3}$	0.620(8)
5.0	2.12(3)	0*	$2.0(1) \times 10^{-3}$	0.634(8)
5.5	1.92(3)	0*	$1.7(1) \times 10^{-3}$	0.631(7)
6.0	1.63(4)	0.024(9)	$1.1(1) \times 10^{-3}$	0.607(9)
6.5	1.69(2)	0*	$1.7(1) \times 10^{-3}$	0.645(7)
7.0	1.56(3)	0*	$1.5(1) \times 10^{-3}$	0.649(9)
7.5	1.51(4)	0*	$1.7(2) \times 10^{-3}$	0.66(1)
8.0	1.35(2)	0.002(10)	$1.24(6) \times 10^{-3}$	0.647(7)
8.5	1.27(3)	0*	$1.2(1) \times 10^{-3}$	0.65(1)
9.0	1.22(3)	0*	$1.2(1) \times 10^{-3}$	0.66(1)
9.5	1.14(2)	0.009(9)	$1.13(7) \times 10^{-3}$	0.650(8)
10.0	1.17(4)	0*	$1.5(2) \times 10^{-3}$	0.67(2)
10.5	1.06(2)	0.009(9)	$1.14(8) \times 10^{-3}$	0.655(9)
11.0	0.99(3)	0.02(1)	$1.0(1) \times 10^{-3}$	0.65(1)
11.5	0.93(3)	0.01(2)	$8.8(9) \times 10^{-4}$	0.65(2)
12.0	0.99(2)	0*	$1.4(1) \times 10^{-3}$	0.675(9)
13.0	0.87(2)	0.02(1)	$1.07(9) \times 10^{-3}$	0.66(1)
14.0	0.76(1)	0.02(1)	$7.4(5) \times 10^{-4}$	0.64(1)
15.0	0.80(2)	0.01(1)	$1.2(1) \times 10^{-3}$	0.67(1)
16.0	0.70(2)	0.02(1)	$8.5(9) \times 10^{-4}$	0.66(1)
17.0	0.63(2)	0.03(1)	$6.9(8) \times 10^{-4}$	0.63(2)
18.0	0.62(3)	0.02(2)	$8(1) \times 10^{-4}$	0.65(3)
19.0	0.53(1)	0.041(9)	$5.2(4) \times 10^{-4}$	0.61(2)
20.0	0.52(2)	0.04(1)	$5.4(7) \times 10^{-4}$	0.60(3)
21.0	0.60(3)	0.008(14)	$1.2(3) \times 10^{-3}$	0.69(2)
22.0	0.53(1)	0.016(9)	$6.8(7) \times 10^{-4}$	0.66(2)
23.0	0.46(1)	0.033(8)	$4.3(4) \times 10^{-4}$	0.61(2)
24.0	0.51(1)	0.014(7)	$7.8(8) \times 10^{-4}$	0.66(1)
25.0	0.44(1)	0.031(6)	$4.5(3) \times 10^{-4}$	0.60(2)
26.0	0.433(8)	0.039(7)	$4.3(3) \times 10^{-4}$	0.57(2)

27.0	0.407(7)	0.052(5)	$3.5(2) \times 10^{-4}$	0.51(2)
28.0	0.368(5)	0.063(6)	$2.2(1) \times 10^{-4}$	0.42(2)
29.0	0.355(6)	0.065(9)	$1.7(1) \times 10^{-4}$	0.37(3)
30.0	0.343(2)	0.069(4)	$1.21(5) \times 10^{-4}$	0.30(2)
32.0	0.314(3)	0.069(9)	$5.5(4) \times 10^{-5}$	0.20(3)
34.0	0.294(3)	0.07(1)	$2.8(3) \times 10^{-5}$	0.12(4)
36.0	0.279(2)	0.08(2)	$1.4(2) \times 10^{-5}$	0.08(5)
38.0	0.267(2)	0.07(6)	$7(3) \times 10^{-6}$	0.07(8)

* fixed at $0 \text{ cm}^3 \text{ mol}^{-1}$

1. I. Aratani, Y. Horii, D. Takajo, Y. Kotani, H. Osawa and T. Kajiwara, *J. Mater. Chem. C*, 2023, **11**, 2082-2088.
2. D. Aravena, F. Neese and D. A. Pantazis, *J. Chem. Theory Comput.*, 2016, **12**, 1148-1156.
3. F. Weigend and R. Ahlrichs, *Phys. Chem. Chem. Phys.*, 2005, **7**, 3297-3305.